TENSILE AND COMPRESSIVE MECHANICAL BEHAVIOR OF IM7/PETI-5 AT CRYOGENIC TEMPERATURES

Karen S. Whitley

Thesis submitted to the faculty of the Virginia Polytechnic Institute and State University in partial fulfillment of the requirements for the degree of

Master of Science
in
Engineering Mechanics

Scott Case, Co-chair

Thomas S. Gates, Co-chair

Richard Barnwell

October 24, 2002
Hampton, VA

Keywords: polymer matrix composites, cryogenic, aging, residual properties

TENSILE AND COMPRESSIVE MECHANICAL BEHAVIOR OF IM7/PETI-5 AT CRYOGENIC TEMPERATURES

Karen S. Whitley

(ABSTRACT)

In order for future space transportation vehicles to be considered economically viable, the extensive use of lightweight materials is critical. For spacecraft with liquid fueled rocket engines, one area identified as a potential source for significant weight reduction is the replacement of traditional metallic cryogenic fuel tanks with newer designs based on polymer matrix composites. For long-term applications such as those dictated by manned, reusable launch vehicles, an efficient cryo-tank design must ensure a safe and reliable operating environment. To execute this design, extensive experimental data must be collected on the lifetime durability of PMC's subjected to realistic thermal and mechanical environments. However, since polymer matrix composites (PMC's) have seen limited use as structural materials in the extreme environment of cryogenic tanks, the available literature provides few sources of experimental data on the strength, stiffness, and durability of PMC's operating at cryogenic temperatures.

It is recognized that a broad spectrum of factors influence the mechanical properties of PMC's including material selection, composite fabrication and handling, aging or preconditioning, specimen preparation, laminate ply lay-up, and test procedures. It is the intent of this thesis to investigate and report performance of PMC's in cryogenic environments by providing analysis of results from experimental data developed from a series of thermal/mechanical tests. The selected test conditions represented a range of exposure times, loads and temperatures similar to those experienced during the lifetime of a cryogenic, hydrogen fuel tank. Fundamental, lamina-level material properties along with properties of typical design laminates were measured, analyzed,

and correlated against test environments. Material stiffness, strength, and damage, will be given as a function of both cryogenic test temperatures and pre-test cryogenic aging conditions.

This study focused on test temperature, preconditioning methods, and laminate configuration as the primary test variables. The material used in the study, (IM7/PETI-5), is an advanced carbon fiber, thermoplastic polyimide composite.

DEDICATION

This thesis is dedicated to my children:

Justin and Megan

ACKNOWLEDGMENTS

Dr. Thomas S. Gates for his many, many hours of consulting, guidance, and support, and for his endless endurance of my complaints and whining.

Dr. Richard Barnwell for going above and beyond the call of duty to ensure that at least half of my courses were offered by Virginia Tech through VCES even if it meant teaching the course himself.

Dr. Scott Case for agreeing to be the chairman of my advising committee, and his committed support in advising me on course work, and profuse willingness to help me with anything I needed.

Lisa Hawks, Everitt Brown, and Ed Townsley for their invaluable technical support in the lab.

Dr. Damodar Ambur, and Dr. Ivatury Raju, my current and former branch head, for their encouragement and support in my pursuit of a Masters degree.

No words can express the honor that Rick, my husband, deserves for loving me through all the years of my education.

The work described in this thesis was performed at NASA Langley Research Center, Hampton, VA 23681-0001.

TABLE OF CONTENTS

LIST OF TABLES

LIST OF FIGURES

LIST OF SYMBOLS

°C	Degrees Centigrade
°F	Degrees Fahrenheit
scc/s/in^2	Standard cubic centimeters per second per square inch
T_g	Glass transition temperature
Tan δ	Loss modulus divided by storage modulus
mm	millimeter
cm	centimeter
µmm/mm-°C	micro-millimeters per millimeters per degrees Centigrade
E_x, E_y	Young's modulus in x-y coordinate directions
E_1, E_2	Young's modulus in principal material directions
G_{ij}	Shear modulus in the i-j plane
σ_x	Longitudinal stress
σ_1, σ_2	Stress in principal material directions
σ_{ij}	Stress matrix elements
ε_x, ε_y, γ_{xy}	Strain in x-y coordinate directions
ε_1, ε_2, γ_{12}	Strain in principal material directions
ε_{ij}	Strain matrix elements
µε	Microstrain
θ	Angle of rotation
ν_{ij}	Poisson's ratio for strain in the j-direction when stressed in the i-direction
S_{ij}	Compliance matrix elements
Q_{ij}	Reduced stiffness matrix elements
$\overline{Q}_{ij}$	Transformed reduced stiffness matrix elements
$[T_\sigma]$	Stress transformation matrix

$[T_\varepsilon]$	Strain transformation matrix
$\eta_{ij,i}$	Coefficient of mutual influence
ε_x^o, ε_y^o, γ_{xy}^o	Middle surface strains
κ_x, κ_y, κ_{xy}	Middle surface curvatures
N_x, N_y, N_{xy}	Resultant forces
M_x, M_y, M_{xy}	Resultant moments
h	Laminate plate thickness
A_{ij}	Extensional stiffness matrix elements
B_{ij}	Coupling stiffness matrix elements
D_{ij}	Bending stiffness matrix elements
t_k	Thickness of the k^{th} layer
$\overline{z}_k$	Distance to the centroid of the k^{th} layer
α_1, α_2	Coefficients of thermal expansion in principal material directions
$\alpha_x, \alpha_y, \alpha_{xy},$	Coefficients of thermal expansion in x-y coordinate directions
ΔT	Temperature difference

1. INTRODUCTION

A common damage mode of PMC's is matrix cracking, which may lead to delamination and ultimately failure [1]. Thermal residual stresses due to the curing process, loading mode, and exposure time at temperatures are among the many factors that can influence the development of microcrack damage. Cross-ply laminates are especially susceptible to transverse matrix cracking leading to a reduction in composite stiffness [2]. Even if microcrack density is not sufficient to diminish structural integrity, the mere presence of microcracks leads to the risk of permeation. Leakage of cryogenic fluids is among the greatest concerns in the utilization of PMC's for crogenic-fuel tanks.

Investigation of the mechanical properties of PMC's under cryogenic environments is essential before proceeding with the basic design concepts of PMC cryo-tanks. Engineering design data on composites for use at cryogenic temperatures are limited, forcing difficult design decisions and leaving room for uncertainties. Complete material characterization is time-consuming and expensive. The experimental data of cryogenic mechanical properties are often obtained for specific discrete temperatures such as LN_2 (-196°C) or LHe (-269°C) conditions. Replicate testing in itself, at both cryogenic temperatures, is also time-consuming and expensive. If there is not significant difference in properties at the two temperatures, then testing at liquid helium temperature may be eliminated, thus saving considerable time and expense.

When designing a structure, the loading mode and direction are important concerns. If both tension and compression loading occur, then both tension and compression design data are needed. However, if temperature dependent properties of PMC's under tension correlate to compression properties, design and analysis can be based on tension data, thus eliminating the expense of replicating a test matrix in multiple loading modes.

It was the objective of this thesis study to investigate the effects of cryogenic temperatures on a polymer matrix composite composed of an intermediate modulus carbon fiber with a

thermoplastic polyimide matrix. The effects of aging with and without a static load in an isothermal cryogenic environment were observed. It was also the intent to determine if the aging environment leads to microcrack damage. Another goal was to determine if tension and compression properties resulted in similar trends to each other at cryogenic temperatures.

Compressive and tensile modulus and strength were measured at room temperature, –196°C, and –269°C on five different specimen ply laminates: $[0]_{12}$, $[90]_{12}$, $[\pm45]_{3S}$, $[\pm25]_{3S}$ and $[45,90_3,-45,0_3,-45,90_3,45]$. One group of specimens that were not aged provided baseline properties. Specimens in a second group were preconditioned by being isothermally aged for 576 hours at –184°C in an unloaded state. A third group of corresponding coupons were mounted in constant displacement fixtures such that a constant uniaxial strain was applied to the specimens for 576 hours at –184°C. Analysis of the measured properties indicated that cryogenic temperatures could have an appreciable influence on strength and stiffness. Residual stress calculations based on lamination theory showed that the transverse tensile ply stresses could exceed allowable levels for cryogenic test temperatures. Microscopic examination of the surface morphology showed evidence of degradation along the exposed edges of the material due to aging at cryogenic temperatures. The application of this data may be used to assist in the materials down select and design of cryogenic fuel tanks for future reusable space vehicles.

2. BACKGROUND

The future of space transportation vehicles may well rely on the economic feasibility of Reusable Launch Vehicles (RLV). As the demands on performance increase for RLV's, the need for efficient, lighter weight structures will also continue to increase. Using PMC's for fuel tank construction is a demanding application for PMC's because a typical cryogenic fuel tank wall must carry structural and pressure loads while safely operating over an extremely wide temperature range (e.g. –250°C to +120°C) for the lifetime of the vehicle. For a launch vehicle to get to orbit and deliver a substantial payload, it must be 90 percent propellant by weight at liftoff. Only 1 percent is for payload, and 9 percent for the total gross liftoff weight remains for

the entire vehicle mass [3]. McDonnell Douglas flew the DC-X in 1993, the first reusable rocket with a cryogenic fuel tank made with PMC's. Then as part of NASA's reusable launch vehicle program, the DC-X was reconfigured into the DC-XA, a suborbital-demonstration vehicle. Because the need to reduce the weight was so great, the development of the DC-XA incorporated lightweight composites throughout its structure. The largest single structure on the vehicle was the unlined hydrogen fuel tank. Thus, the greatest reduction in weight could be accomplished by making the cryogenic fuel tanks out of polymer matrix composites (PMC) instead of the traditional aluminum materials. The all-composite liquid-hydrogen fuel tank was designed as an unlined, unstiffened cylinder measuring approximately 2.4 m in diameter and 4.8 m long and weighed 67 percent of the aluminum tank weight (1908 pounds vs. 2851 pounds). The DC-XA was successfully flown in 1996, and the tank performed as expected in both ground and flight tests. Although long-term use of the tank was not investigated, short-term testing indicated that permeation resistance and structural load carrying capability met the design requirements [3].

From a durability perspective, the primary design criteria of the PMC material in a cryo-tank is to retain mechanical properties within allowable limits over the life-time of the tank while minimizing loss of cryogenic fuel due to permeation or leakage through the tank wall. These design criteria led to research that focused on the feasibility of polymeric composites as applicable materials in cryogenic propellant tanks. In 1994, Robinson [4] performed hydrogen permeation studies of composite materials at cryogenic temperatures for use in the National Aerospace Plane (NASP), also known as the X-30, and other single-stage-to-orbit (SSTO) vehicles. The allowable permeation rate was calculated to be in the range of 10^{-4} to 10^{-3} scc/s/in^2. Five resins that were found to have superior permeation resistance were then subjected to tensile testing at –269°C (LHe temperature) before and after thermo-mechanical cycling. Robinson's results showed minimal change in cryogenic tensile strength, and concluded that the concept of composite cryogenic tanks was a viable option.

Others have performed additional feasibility studies. Callaghan, [5] studied the potential advantages of different resins and fibers for use in composite structures at cryogenic

temperatures. Callaghan found that high molecular weight thermosets resulted in high strength and thermal stability, however their formulation resulted in limited toughness, which may lead to the susceptibility of delaminating during low velocity impact. Conversely, thermoplastics demonstrated high toughness, ease of processability, and low hydrogen permeability. Among candidate fibers, graphite had the greatest strength and stiffness, but also had the largest CTE mismatch between the fiber and the matrix. A feasibility study performed by Morino [6] et. al. included conducting cryogenic testing on a bismaleimide and a thermoplastic matrix. They found that the thermoplastic materials in the study tended to decrease in tensile strength as temperature decreased. However, the bismaleimide, which is a thermoset, had maximum strength at cryogenic temperatures. A possible reason for this tendency could be due to the large thermal strains that are developed in the thermoplastic matrix resin during the manufacturing process of a quasi-isotropic lay-up configuration. The materials that were thermally cycled from 100°C to -160°C showed no visual damage or microcracking. Thermal contraction of the materials in the fiber direction was very small whereas the thermal contraction in the direction transverse to the fiber reached 0.6% at liquid helium temperatures. This large difference in thermal contraction was considered as the source of internal thermal stresses.

In the work by Pannkoke and Wagner [7], fatigue tests were performed on 16-ply-unidirectional thermoplastic composites at –196°C. The fatigue strength was found to be only 60% of the static strength at 10^6 cycles. In this work, it was recognized that the fiber-matrix bond had little influence on fatigue resistance of the composites, but that large thermal stresses degraded the fatigue performance. The duroplastic matrix composite (EP Rigidite R5212/G30-500) used in their study, showed multiple transverse crack propagation, but good fatigue behavior. The thermoplastic matrix composite showed little crack formation and lower fatigue endurance.

In a series of articles by Ahlborn, [8], [9] static and cyclic thermal/mechanical tests were performed on unidirectional and cross-ply thermoplastic composites, HTA/7/PC and AS4/PEEK. Isothermal tests were performed at 23°C, –196°C, and –269°C and cyclic thermal tests were performed between –196°C and 23°C. Strength, damage, and fatigue life were measured for all test conditions. It was found that the effects of temperature on static strength were largely

related to the matrix dominated properties, shear and transverse tension, and that increases in matrix dominated strength as temperature decreased could be offset by the development of thermal-stress induced cracks. As in previous studies, the fatigue life was reduced as the test temperature was decreased. The thermoplastic composites had a higher sensitivity to tension-tension loads at low temperatures than the epoxy composites. This may have been from the development of thermal prestresses in the thermoplastics between the unidirectional layers and the angle-ply layers due to expansion mismatch and high production temperatures.

For amorphous and crystalline polymeric materials, Perepechko [10] provided details on a number of non-mechanical properties including thermal expansion, thermal conductivity, as well as viscoelastic or dynamical mechanical properties. From these studies, it was clear that many of the polymer properties are not linear with respect to temperature change from room temperature to close to absolute zero.

More recently, a compilation of test data for several PMC material systems [11] showed that in general, tensile modulus, tensile strength, and compressive strength all increased as the test temperature was decreased from 23°C to –269°C. Once again, it was found that thermal stresses had a large influence on behavior and that the sensitivity of matrix-dominated properties to temperature can be used to help explain the stress-strain response of laminated composites. Of these matrix-dominated properties, transverse ply strength may play a critical role in the development and growth of residual stress induced matrix cracks. The range of thermal/mechanical loading over which steady-state matrix cracking may occur was recently investigated by Schoeppner et. al. [12]. They experimentally measured the first-ply-failure (FPF) stress, defined as the first occurrence of a ply level transverse crack, at room temperature and –196°C on three different lay-ups of IM7/977-3. It was found that the in-situ FPF stress (ply transverse crack strength) decreases for increasing effect ply thickness, so ply grouping should be avoided. The average FPF was lower at the cryogenic temperature than it was at room temperature.

Additional studies related to matrix crack development in PMC's due to cryogenic temperature exposure can be found in reference [2] where carbon fiber/epoxy composites were cryogenically cycled between room temperature and liquid nitrogen temperature. It was found that composites containing higher modulus fibers were more prone to microcracking, because the higher tensile modulus fibers have an increased negative longitudinal coefficient of thermal expansion (CTE). Thus, the larger difference in CTE between the matrix and fiber increased the thermal stresses at low temperatures. The microcrack density was also influenced by the chemical structure of the matrix material such that an increased backbone flexibility caused an increase in microcrack density. However, the presence of a rubber toughener prevented the formation of microcracks in all the laminates studied.

3. MATERIAL SYSTEM

The PMC material used in this study, IM7/PETI-5, consisted of a high strength, intermediate modulus, continuous carbon fiber in a thermoplastic polyimide matrix. All test materials were laminated composites panels fabricated at the NASA Langley Research Center. These composite panels consisted of unidirectional and angle-ply laminates, ($[0]_{12}$, $[90]_{12}$, $[\pm25]_{3S}$, $[\pm45]_{3S}$), and a 13-ply orthotropic laminate ($[45/90_3/-45/0_3/-45/90_3/45]$). Figure 1 provides a schematic illustrating the coordinate system for the fiber orientations relative to the specimen dimensions. The subscript 12 in $[0]_{12}$ and $[90]_{12}$ indicates that there are 12 plies in those laminates. The subscript 3S in $[\pm25]_{3S}$ and $[\pm45]_{3S}$ indicates that the pattern is repeated 3 times, and is then laid-up symmetrically. For example, $[\pm45]_{3S}$ is shorthand notation for [+45/-45/+45/-45/+45/-45/-45/+45/-45/+45/-45/+45], which represents a 12-ply laminate.

These lay-ups were chosen to provide basic lamina-level material constants and in the case of the $[\pm25]_{3S}$ and $[45/90_3/-45/\bar{0}_3]_S$ –ply laminates, to be representative of a composite wall in a typical cryogenic propellant tank. For a cryogenic tank, the orientation of the 0°ply in the $[45/90_3/-45/\bar{0}_3]_S$ laminate would be in the longitudinal axis direction of the tank.

All composite panels were fabricated by hand lay-up. The bagging and cure processes employed were consistent with standard practices. A full vacuum was applied to the bagged panel during the entire cure cycle. The cycle started with a ramp to 260°C at 5°C/minute. After a 1-hour hold at 260°C, the autoclave was pressurized to 1480 kPa at 170 kPa/minute while the temperature was ramped to 370°C at 5°C/minute. The temperature was held at 370°C for 1 hour. The pressure was maintained until the temperature cooled to 38°C. Through-transmission, ultrasonic inspection indicated that there were no significant internal anomalies in any of the panels. The 12 x 12 inch panels were cut into appropriate size test coupons. The glass transition temperature (T_g) of the as-received composite material was 267°C as measured by the peak in the Tan δ curve of tests run in a dynamic mechanical analysis (DMA) test [13].

4. EXPERIMENTAL APPROACH

4.1 Material Aging Conditions

Material characterization including tensile and compressive residual property measurements was performed on three groups of IM7/PETI-5. The first group represented material without pre-conditioning, which distinguished the baseline values, and provided fundamental material properties. The second group was subjected to long-term exposure at a cryogenic temperature (aging time of 576 hours for –184°C) in an unconstrained state. The third group was subjected to the same long-term exposure at the same cryogenic temperature (aging time of 576 hours for –184°C) while being statically loaded. Comparing test data from the not aged group against the unconstrained and constrained specimens provided an understanding of material behavior as a function of aging and load conditions.

For group 3, the constrained specimens, a unique test fixture that was developed under the NASA High Speed Research Program [14], was used to produce a constant strain condition during the aging phase. Each fixture, shown in figure 2, was constructed of Invar material (CTE

= 1.4 μmm/mm – °C) and could accommodate two rectangular specimens. Each specimen was individually preloaded to the desired strain level by compressing a series of spring-type washers that react against the frame and put the specimen into tension. As the specimen was preloaded and the washers were tightened, the preload strain level in the specimen was monitored with a longitudinal extensometer mounted on the specimen. The high stiffness of the fixture relative to the test specimen and the low CTE of the Invar material ensured a constant strain condition over the entire aging period.

The preload strain level, given in table 1, was determined based on design allowables. A strain range of 0.3% (3000 microstrain) to 0.4% (4000 microstrain) is considered to be reasonable as a design allowable for most composite structural applications. The room temperature stress-strain curves for each group of ply lay-ups (figure 3) were used to ensure that this strain range was less than 50% of the failure strain, and was well within the linear region of the stress-strain curve. Figure 4 shows the same stress-strain curves on a smaller scale to accentuate the linear region. It was determined that 4000 microstrain met the above criteria and was easily achievable by the constant-strain test fixture pictured in figure 2. However, 4000 microstrain was beyond the linear region of the stress-strain curve of the $[\pm 45]_{3S}$ –ply laminate. Even though 4000 microstrain may not have been enough to induce damage in a $[\pm 45]_{3S}$ –ply laminate, 3000 microstrain was chosen as the pre-strain level for that laminate so as remain within the linear region. Due to the high stiffness of the $[0]_{12}$ –ply laminate, 3000 microstrain was the maximum strain achievable by the constant-strain test fixture. Because 3000 microstrain was greater than 50% of the failure strain of the $[90]_{12}$ –ply laminates, an attempt was made to apply a pre-strain level of 2000 microstrain to the $[90]_{12}$ –ply laminates, but they still failed prematurely during or shortly after mounting into the constant strain fixtures.

A large cryo-chamber (figure 5) that is a top-loading deep-freezer style with interior dimensions measuring 48 cm wide x 178 cm long x 63 cm deep was used to age specimens. During the course of an aging phase, thirteen constant strain fixtures, each holding two constrained coupons (group 3), were placed in the bottom of the cryo-chamber. Corresponding sets of unconstrained

coupons (group 2), arranged side-by side in wire baskets were also placed in the bottom of the chamber. The temperature-programmable cryo-chamber used a refrigeration system to cool from room temperature to –73°C at a rate of 8.2°C/hour. Subsequently, the chamber used liquid nitrogen to achieve the final aging temperature of –184°C at a much faster rate of 3.7°C/minute. Once reaching –184°C, the chamber maintained that constant temperature for an aging time of 576 hours.

4.2 Post-aging Test Matrix

All specimens were cut to appropriate dimensions and dried at 121°C for 24 hours to remove any residual moisture prior to the aging process. Upon completion of aging, the specimens repeated the drying cycle to remove moisture from condensation that resulted from the cooling process. Specimens then remained in a dessicator until tested. The three groups of specimens were then tested for residual strength and stiffness in tension and compression at room temperature, -196°C, and -269°C, which provided material behavior as a function of test temperature. The complete test matrix including the aging conditions and the residual property tests are shown in table 1. Three replicates were tested at each condition and results of the three were averaged.

5. RESIDUAL PROPERTY TESTING

5.1 Tension Test Procedure

The general set of references for the residual tension test was SACMA SRM 4-88 and ASTM D 3039-76. The residual property tests were performed on a servo-hydraulic test machine using a loading rate of 1.27 mm/min. A schematic of the tensile specimens is detailed in figure 6. The untabbed tensile coupons tested at room temperature were 152 mm x 25 mm, and 38 mm of each end were mounted in hydraulic wedge grips leaving a 76 mm test section. The untabbed 254 mm x 19 mm cryogenic tension coupons were mounted such that 63 mm of each end was gripped between two serrated face-plates leaving a 127 mm test-section. The face-plates were tightened through six hex-head bolts using a hand-held torque wrench. The isothermal cryogenic

conditions at –196°C and –269°C were achieved by immersing the test specimen, grips, and load introduction apparatus into liquid nitrogen or liquid helium respectively. In order to reach thermal equilibrium, the specimen stayed immersed in a constant level of the cryogen for at least 15 minutes prior to mechanical loading.

Stress in the test specimens was calculated using load, as measured by the test machine load cell, divided by the original cross section of the specimen. Failure load was defined as the point of complete loss of load carrying capability. Strain in all the test specimens was measured using an axial extensometer (MTS model 634.11F-21), expect the $[\pm 45]_{3S}$ –ply laminates, which used a combination of the axial extensometer and bonded electrical resistance strain gages (Measurements Group WK-00-250BG-350). Both the extensometers and strain gages were rated for cryogenic temperatures. Because the tests were performed at an isothermal temperature, compensation for temperature variation between the specimen and the measuring devices was easily achieved by zeroing the extensometer and gages after the specimen reached thermal equilibrium. Details on these techniques can be found in [15]. The placement of these sensors on the specimen is shown in figure 6.

5.2 Compression Test Procedure

The compression residual property tests were performed using SACMA recommended method SRM 1-88 and the ASTM D695 references as guides. The compression tests were performed using the same servo-hydraulic test machines that were used for the tension tests. Likewise, the loading rate of 1.27 mm/min was used for the compression tests. The coupons aged in the unloaded state were precisely cut to measure 25 mm x 76 mm, with the ends ground parallel to each other prior to the aging process. Coupons measuring 25 x 254 mm were aged in the constant strain fixtures with an axial load applied. After aging, two compression coupons of length 76 mm were precisely cut from the middle section of the longer 254 mm length. Stacked-rosette-style electrical resistance strain gages bonded to the coupons were used to measure strain in the axial and transverse directions. Measurements Group CEA-06-125WT-350 gages were used for room temperature measurements and Measurements Group WK-06-120WT-350 gages

were used in cryogenic temperature tests. A schematic of the compression specimens is shown in figure 7.

The gauged coupons were placed in the center cut-out section of the compression test fixture as shown in figure 8(a). The cut-out portion in the interior of the fixture allowed room for the gages to measure strain without constraints. The fixture was assembled as shown in the side view of figure 8(b). This end-loaded compression fixture supported the specimen to prevent buckling, and allowed compression failure in the mid-section. The compression apparatus set-up is shown schematically in figure 9. The fixture containing the specimen was placed between the two compression platens. To ensure alignment, the adapter, extension rod, and compression platens were machined such that all ends were parallel to each other, and all threads were drilled concentric about the center of their respective diameters. Four aligning rods were also used to support the bottom plate that was affixed to the bottom compression platen. Distance between compression platens was measured in multiple locations around the circumference of the platens to verify parallelism.

The isothermal cryogenic test conditions at –196°C and –269°C were achieved by immersing the test specimen, test fixture, and load introduction apparatus into liquid nitrogen or liquid helium respectively. In order to reach thermal equilibrium, the specimen stayed immersed in a constant level of the cryogen for at least 15 minutes prior to mechanical loading. Temperature compensation was achieved by zeroing the gages after the specimen reached thermal equilibrium as discussed in the tension procedure section.

6. EXPERIMENTAL RESULTS AND DISCUSSION

6.1 Elastic Constant Calculation

The tensile and compressive elastic properties were calculated according to ASTM D3039-76 and ASTM D695, respectively. The Young's modulus (E) was calculated using equation (1) and a linear regression least squares fit of the stress-strain data in the linear portion of the

longitudinal stress (σ_x) versus the longitudinal strain (ε_x) curve. This linear region of the stress-strain curve was defined as being between 1000$\mu\varepsilon$ and 3000$\mu\varepsilon$ for all test conditions and specimen ply lay-ups. Poisson's Ratio, (ν) given by equation (2), was calculated in the same linear region. Shear modulus (G_{12}) given by equation (3), was calculated for the $[\pm 45]_{3S}$ specimens using the above values for E and ν.

$$E_X = \frac{\sigma_x}{\varepsilon_x} \tag{1}$$

$$\nu_{xy} = -\frac{\varepsilon_y}{\varepsilon_x} \tag{2}$$

$$G_{12} = \frac{E_x}{2\left(1+\nu_{xy}\right)} \tag{3}$$

Elastic modulus and strength results are presented for laminates with $[0]_{12}$, $[\pm 25]_{3S}$, $[45/90_3/-45/\bar{0}_3]_S$, $[90]_{12}$, and $[\pm 45]_{3S}$ -ply stacking sequences. Table 2 and table 3 contain the tensile and compressive elastic modulus, respectively, at the three different test temperatures, for each lay-up for each aging condition. Each value in the table represents the average of three replicates along with the standard deviation. The lamina in-plane stiffness values E_1 and E_2, were calculated directly from stress-strain behavior of the unidirectional laminates, $[0]_{12}$ and $[90]_{12}$, respectively. The laminate stiffness value E_x of the laminates $[\pm 25]_{3S}$ and $[45/90_3/-45/\bar{0}_3]_S$, was calculated from the laminate stress-strain behavior. Lamina in-plane shear modulus G_{12} was calculated indirectly from the stress-strain behavior of the $[\pm 45]_{3S}$.

Measured laminate tensile and compressive strength values are listed in table 4 and table 5, respectively, along with the associated standard deviation. Failure was defined as the point of complete loss of load carrying capability during the test. Due to the nonlinear nature of the stress-strain behavior in $[\pm 45]_{3S}$ laminates, their tensile strength was defined as the initial point of deviation from the nearly horizontal portion of the stress-strain curve as shown in figure 10.

Figures 11-18 present the tensile modulus and strength with the values normalized against the not aged condition tested at room temperature. Likewise, the compressive modulus and strength have been normalized against the not aged condition tested at room temperature in figures 19-26.

6.2 Effect of Temperature on Modulus and Strength

6.2.1 Tension

By examining the results from specimens subjected to not-aged test condition, the effects of temperature on tensile modulus and strength were found. At cryogenic temperatures, the not aged and the aged-without-load group of the fiber dominated laminate $[0]_{12}$ ply laminate experienced only a slight decrease in modulus (figure 11). The strength of the $[0]_{12}$ ply laminate decreased in all three groups (figure 12). The not aged group experienced the greatest decrease in strength of 33% at –196°C.

The shear modulus and longitudinal strength of the matrix dominated $[\pm 45]_{3S}$ –ply laminate increased as the temperature decreased (figure 13 and figure 14). The shear modulus increased by as much as 35% and the strength by as much as 50% when tested at –269°C. The transverse modulus (E_2) showed a slight decline at cryogenic temperatures while the transverse strength dropped by approximately 70% when the temperature was reduced to –269°C. The tensile modulus and strength of the not aged $[45/90_3/-45/\bar{0}_3]_S$ –ply laminates decreased by nearly 20% at –196°C, with some reverse in this decline as the temperature was lowered to –269°C (figure 15 and figure 16). The $[\pm 25]_{3S}$ –ply laminates showed little sensitivity in modulus or strength to cryogenic temperature.

By plotting the strength of all the not-aged laminates on the same graph (figure 27) and normalizing each group of laminates against the room temperature test, it can be seen that the lowest strength doesn't necessarily occur at the lowest test temperature as expected. The $[0]_{12}$,

$[\pm 25]_{3S}$, and the $[45/90_3/-45/\bar{0}_3]_S$ –ply laminates had the lowest strength at –196°C. The fragile $[90]_{12}$ –ply laminates did have the lowest strength at the lowest temperature of –269°C.

6.2.2 Compression

The compressive modulus of the not aged material increased for all laminates due to testing at cryogenic temperatures as shown in figure 28. In most laminates the highest modulus occurred at the lowest test temperature (–269°C). Compressive strength was the greatest at the lowest test temperature (–269°C) for all the laminates as shown in figure 29. However, the $[45/90_3/-45/\bar{0}_3]_S$ and the $[\pm 45]_{3S}$ -ply laminates had the lowest strength at –196°C (figure 29), again demonstrating that the lowest test temperature was not necessarily the worst case. Of all the laminates tested, the $[90]_{12}$ experienced the greatest increase (67%) in strength while the $[\pm 45]_{3S}$ experienced the greatest increase (57%) in modulus due testing at cryogenic temperatures.

6.3 Effect of Aging on Modulus and Strength

6.3.1 Tension

To determine the effects of aging, the not aged condition can be compared to the aged without load and the aged with load conditions. In general aging had very little effect on the tensile modulus of the fiber dominated $[0]_{12}$–ply laminate. Aging did cause a slight increase in tensile strength for the $[0]_{12}$–ply laminate with the most significant change occurring when tested at –269°C after aging with load (figure 12). Aging increased the room temperature shear modulus and strength of the matrix dominated $[\pm 45]_{3S}$ –ply laminate (figure 13 and figure 14).

For the laminate with the ply stacking sequence, $[45/90_3/-45/\bar{0}_3]_S$, aging increased the modulus (figure 15). The largest increase (18%) occurred for the laminate aged with load condition tested at –269°C. Aging also increased the strength of the $[45/90_3/-45/\bar{0}_3]_S$–ply laminate with the most significant increase occurring at the aged with load condition where strength increased relative to the baseline by 21% at –196°C and 11% at –269°C (figure 16). In general, aging decreased the modulus of the $[\pm 25]_{3S}$–ply laminate and had little effect on the laminate strength (figure 17 and

figure 18). From the limited data for the $[90]_{12}$ –ply laminate, it appears that aging had little effect on transverse modulus or strength.

As expected, the standard deviation in strength measurements was more significant than the standard deviation associated with modulus. In part, this is due to strength being a point or single value, whereas modulus is an overall measure of stiffness based on an averaged value of an integrated volume quantity. Also, in most cases, strength is controlled by a point defect. Strength in laminated composites is also more sensitive to the processing, handling, or test parameter variability.

6.3.2 Compression

The compressive modulus and strength of the $[0]_{12}$ –ply laminate were not greatly influenced by aging (figure 19 and figure 20). The matrix dominated $[\pm 45]_{3S}$ –ply laminate showed a decrease in compressive modulus and strength due to aging in most cases, and in general, the modulus decreased more than the strength (figure 21 and figure 22). The compressive modulus of the $[45/90_3/\text{-}45/\bar{0}_3]_S$–ply laminate tended to decrease after aging (figure 23). The compressive strength of the $[45/90_3/\text{-}45/\bar{0}_3]_S$–ply laminate increased due to aging (figure 24). The greatest increase (88%) occurred at –269°C after aging with load, however the standard deviation associated with those strength values was quite high. The room temperature modulus and strength of the $[\pm 25]_{3S}$ –ply laminate were unaffected by aging, however at –196°C both modulus and strength increased due to aging (figure 25 and figure 26). The $[90]_{12}$ –ply laminate was not significantly affected due to aging.

7. PHOTOMICROSCOPY

7.1 Procedure

Before the destructive residual tests, optical examination of the surface morphology of all lay-ups was performed to determine if the exposure conditions generated any microcrack damage during specimen aging. The specimen preparation started prior to aging exposure, where

representative samples were polished along one edge. Sections (2.6 x 1.3 cm) were potted in a clear epoxy mold and were then circulated in an automated polishing wheel at 150 rpm's with an applied weight of 5 pounds per specimen. Consecutive grades of grit paper (600, 800, 1200 grit) were used for the polishing. The specimens received a final polish with a solution of silica alumina suspension fluid. The polished specimen edges were examined for damage (microcracks, delaminations) using optical microscopy, and photomicrographs were taken to establish the baseline condition. After aging exposure, but prior to the destructive residual tests, visual examination of all lay-ups was again performed to determine if the exposure conditions generated any microcracks, damage, or change in surface morphology. A microcrack was defined as a transverse or longitudinal crack, observable under at least 25x magnification, which was at least one ply thickness in length.

7.2 Surface Morphology

Optical examination of surface morphology was intended to provide data on the initiation and growth of any damage that occurred during specimen aging. Photomicrographs representative of the specimen's polished edges before and after aging are shown in figures 30 thru 33. On each figure page, the (a), (b), and (c) are typical of laminates before aging, after aging without load, and after aging with load, respectively. Based on the data in the literature [11], [12], and [2] it was expected that microcrack damage could even occur as a result of the cure process itself when the large change in temperature from the stress-free cure temperature to room temperature would induce intralaminar stresses. However, very few microcracks or similar damage was observed before or after aging in any of the lay-ups. Even though microcracks were not the dominate feature, the surface morphology did show some definite degradation along the exposed edges after aging without load and it appeared that further surface degradation occurred after aging with load. This degradation occurred in all lay-ups and can be described as pitting in the matrix regions. This degradation may have an adverse influence on residual strength due to the increase in possible failure initiation sites.

8. FRACTURE SURFACE

8.1 Tension

The fracture surfaces of each failed specimen were examined for any distinguishing features that could be attributed to test temperature or aging conditions. It was observed that distinguishing characteristics in the fracture surfaces were not due to aging. However, comparing the room temperature tests and the cryogenic tests brought about the greatest distinction in the appearance of the fracture. There were no discernable differences between the specimens tested at -196°C and -269°C.

The fracture surface of $[45/90_3/-45/\bar{0}_3]_S$ laminate tested at room temperature and -196°C are shown in figures 34(a) and 34(b), respectively. The fractured edge of the $[45/90_3/-45/\bar{0}_3]_S$ laminate tested at room temperature appeared more jagged such that the ±45° laminae were more apparent. The $[45/90_3/-45/\bar{0}_3]_S$ laminate tested at -196°C had a fracture surface that failed perpendicular to the direction of the applied load. The $[\pm25]_{3S}$ laminates tested at room temperature (figure 35(a)) displayed irregular fracture surfaces, whereas the $[\pm25]_{3S}$ laminates tested at -196°C (figure 35(b)) displayed a very clean-cut failure along either/or a ±25° direction. All the $[0]_{12}$ laminates failed by splitting along the 0° direction. The failure of the –196°C $[0]_{12}$ laminates were characterized by only a few splits through the thickness as compared to the room temperature $[0]_{12}$ laminates which displayed a more catastrophic splintering as shown in figures 36(a) and (b). In general, the failure of the $[45/90_3/-45/\bar{0}_3]_S$, $[\pm25]_{3S}$, and the $[0]_{12}$ laminates at cryogenic temperatures could be described as "clean breaks," as opposed to the irregular fragmented breaks that occurred at room temperature. This indicates a more brittle fracture at cryogenic temperatures and a more ductile fracture at room temperature. There was no difference in the fracture surface of the $[90]_{12}$ laminates which all failed straight across the width of the specimen in the 90° direction regardless of the test temperature. Due to the nonlinear stress-strain behavior of the $[\pm45]_{3S}$, loading to the point of fracture did not always occur.

8.2 Compression

The fracture surfaces of the specimens tested in compression did not show any differences due to test temperature or aging conditions. Each set of laminate configurations displayed unique failure characteristics as expected. In all cases, failure occurred contiguously above or below the strain gage section. The $[0]_{12}$ laminate compression failures did not split along the length as in the tension tests. Instead, the fracture surface could be described as having short broom-like appearance along the failed edge (figure 37). The $[90]_{12}$ laminates failed with a clean-cut beveled edge across the width (figure 38). The $[\pm 25]_{3S}$ laminates failed sharply along a ±25° angle ply from any one of the four corners of the specimen (figure 39). The $[45/90_3/-45/\bar{0}_3]_S$, failed straight across the width of the specimen with the fracture surface having a crushed appearance (figure 40). The $[\pm 45]_{3S}$ was the only laminate to show some trend toward different failure characteristics due to test temperature. As in the case of the tension tests, because of the non-linearity of the $[\pm 45]_{3S}$, compression tests did not always give way to a complete fracture across the width of the specimen. The failure at room temperature was more of a delamination between the plies as shown in figure 41(a). If complete across-the-width-failure occurred, it was most likely at the cryogenic temperatures (figure 41(b)).

9. RESIDUAL STRESS ANALYSIS

9.1 Lamination Theory Background

Classical Lamination Theory (CLT) utilizes the elastic properties of the lamina to predict theoretical laminate properties. The variations of stress and strain through the thickness of the laminate can be determined and the laminate stiffness can be derived for a laminate composed of arbitrary fiber orientations [16]. The Cartesian coordinate system is most often used to define directions, such that the x-axis is the direction of the applied load, and the y-axis is the direction transverse to the load. The 1-axis is in the direction of the fiber in a unidirectional composite, and the 2-axis is the direction transverse to the fiber. These coordinate systems are shown in figure 1.

The stress-strain relationships in principal material coordinates for a lamina of an orthotropic material under plane stress is given by equation 4,

$$\begin{Bmatrix} \varepsilon_{11} \\ \varepsilon_{22} \\ \gamma_{12} \end{Bmatrix} = \begin{bmatrix} S_{11} & S_{12} & S_{16} \\ S_{21} & S_{22} & S_{26} \\ S_{61} & S_{62} & S_{66} \end{bmatrix} \begin{Bmatrix} \sigma_{11} \\ \sigma_{22} \\ \sigma_{12} \end{Bmatrix} \tag{4}$$

where

$$\begin{aligned} S_{11} &= \frac{1}{E_1} \\ S_{12} &= -\frac{\nu_{12}}{E_1} \\ S_{22} &= \frac{1}{E_2} \\ S_{66} &= \frac{1}{G_{12}} \\ S_{16} &= S_{26} \end{aligned} \tag{5}$$

The E_1 and E_2 equals Young's moduli in the 1 and 2 directions, respectively, and ν_{12} is Poisson's ratio for transverse strain in the 2-direction when stressed in the 1-direction. G_{12} is the shear modulus in the 1-2 plane. The equations for Young's moduli, Poisson's ratio, and shear modulus are given by (6), (7), and (8), respectively.

$$E_1 = \frac{\sigma_1}{\varepsilon_1} \qquad \text{and} \qquad E_2 = \frac{\sigma_2}{\varepsilon_2} \tag{6}$$

$$\nu_{12} = -\frac{\varepsilon_2}{\varepsilon_1} \tag{7}$$

$$G_{12} = \frac{E_x}{2\left(1+\nu_{xy}\right)} \tag{8}$$

Noting that there are four independent elastic constants, and by inverting equation 4, results in equation 9.

$$\begin{Bmatrix} \sigma_{11} \\ \sigma_{22} \\ \sigma_{12} \end{Bmatrix} = \begin{bmatrix} \dfrac{E_1}{1-\nu_{12}\nu_{21}} & \dfrac{\nu_{12}E_2}{1-\nu_{12}\nu_{21}} & 0 \\ \dfrac{\nu_{12}E_2}{1-\nu_{12}\nu_{21}} & \dfrac{E_2}{1-\nu_{12}\nu_{21}} & 0 \\ 0 & 0 & G_{12} \end{bmatrix} \begin{Bmatrix} \varepsilon_{11} \\ \varepsilon_{22} \\ \gamma_{12} \end{Bmatrix} \tag{9}$$

The 3 x 3 matrix in the above equation is usually denoted as

$$[Q] = \begin{bmatrix} Q_{11} & Q_{12} & 0 \\ Q_{12} & Q_{22} & 0 \\ 0 & 0 & Q_{66} \end{bmatrix} \tag{10}$$

in which Q_{ij} are called reduced stiffnesses. In stress analyses, sometimes the x-y coordinate system does not coincide with the material principal axis-1 and axis-2 as illustrated in figure 1. The two sets of stress components with respect to these two coordinate systems are related by the reduced transformation matrix $[T_\sigma]$, such that

$$\begin{Bmatrix} \sigma_{11} \\ \sigma_{22} \\ \sigma_{12} \end{Bmatrix} = [T_\sigma] \begin{Bmatrix} \sigma_{xx} \\ \sigma_{yy} \\ \sigma_{xy} \end{Bmatrix} \tag{11}$$

where

$$[T_\sigma] = \begin{bmatrix} \cos^2\theta & \sin^2\theta & 2\sin\theta\cos\theta \\ \sin^2\theta & \cos^2\theta & -2\sin\theta\cos\theta \\ -\sin\theta\cos\theta & \sin\theta\cos\theta & \cos^2\theta - \sin^2\theta \end{bmatrix} \tag{12}$$

In the same manner, the strains with respect to the two coordinate systems are related by

$$\begin{Bmatrix} \varepsilon_{11} \\ \varepsilon_{22} \\ \gamma_{12} \end{Bmatrix} = [T_\varepsilon] \begin{Bmatrix} \varepsilon_{xx} \\ \varepsilon_{yy} \\ \gamma_{xy} \end{Bmatrix} \tag{13}$$

where

$$[T_\varepsilon] = \begin{bmatrix} \cos^2\theta & \sin^2\theta & \sin\theta\cos\theta \\ \sin^2\theta & \cos^2\theta & -\sin\theta\cos\theta \\ -2\sin\theta\cos\theta & 2\sin\theta\cos\theta & \cos^2\theta - \sin^2\theta \end{bmatrix} \tag{14}$$

Using the transformation matrices $[T_\sigma]$ and $[T_\varepsilon]$, we have

$$\begin{Bmatrix} \sigma_{xx} \\ \sigma_{yy} \\ \sigma_{xy} \end{Bmatrix} = [T_\sigma]^{-1} \begin{Bmatrix} \sigma_{11} \\ \sigma_{22} \\ \sigma_{12} \end{Bmatrix} = [T_\sigma]^{-1}[Q] \begin{Bmatrix} \varepsilon_{11} \\ \varepsilon_{22} \\ \gamma_{12} \end{Bmatrix} = [T_\sigma]^{-1}[Q][T_\varepsilon] \begin{Bmatrix} \varepsilon_{11} \\ \varepsilon_{22} \\ \gamma_{12} \end{Bmatrix} \tag{15}$$

Thus, the stress-strain relations for the state of plane stress parallel to the x-y (1-2) plane become

$$\begin{Bmatrix} \sigma_{xx} \\ \sigma_{yy} \\ \sigma_{xy} \end{Bmatrix} = [\overline{Q}] \begin{Bmatrix} \varepsilon_{xx} \\ \varepsilon_{yy} \\ \gamma_{xy} \end{Bmatrix} \tag{16}$$

where

$$[\overline{Q}] = [T_\sigma]^{-1}[Q][T_\varepsilon] = [T_\varepsilon]^T[Q][T_\varepsilon] \tag{17}$$

The stress-strain relations in an arbitrary (x,y) coordinate system can be expressed in apparent engineering moduli as

$$\begin{Bmatrix} \varepsilon_{xx} \\ \varepsilon_{yy} \\ \gamma_{xy} \end{Bmatrix} = \begin{bmatrix} \frac{1}{E_x} & -\frac{\nu_{yx}}{E_y} & \frac{\eta_{xy,x}}{E_x} \\ -\frac{\nu_{xy}}{E_x} & \frac{1}{E_y} & \frac{\eta_{xy,y}}{E_y} \\ \frac{\eta_{xy,x}}{E_x} & \frac{\eta_{xy,y}}{E_y} & \frac{1}{G_{xy}} \end{bmatrix} \begin{Bmatrix} \sigma_{xx} \\ \sigma_{yy} \\ \sigma_{xy} \end{Bmatrix} \tag{18}$$

For a single layer of orthotropic material, the apparent engineering moduli can be expressed in terms of the principal engineering constants as:

$$\frac{1}{E_x} = \frac{1}{E_1}\cos^4\theta + \left(\frac{1}{G_{12}} - \frac{2\nu_{12}}{E_1}\right)\sin^2\theta\cos^2\theta + \frac{1}{E_2}\sin^4\theta \tag{19}$$

$$\nu_{xy} = E_x\left[\frac{\nu_{12}}{E_1} - \left(\frac{1}{E_1} + \frac{1}{E_2} + \frac{2\nu_{12}}{E_1} - \frac{1}{G_{12}}\right)\sin^2\theta\cos^2\theta\right] \tag{20}$$

$$\frac{1}{E_y} = \frac{1}{E_1}\sin^4\theta + \left(\frac{1}{G_{12}} - \frac{2\nu_{12}}{E_1}\right)\sin^2\theta\cos^2\theta + \frac{1}{E_2}\cos^4\theta \tag{21}$$

$$\frac{1}{G_{xy}} = \frac{1}{G_{12}} + 4\left(\frac{1}{E_1} + \frac{1}{E_2} + \frac{2\nu_{12}}{E_1} - \frac{1}{G_{12}}\right)\sin^2\theta\cos^2\theta \tag{22}$$

$$\eta_{xy,x} = E_x\left[\left(\frac{2}{E_1} + \frac{2\nu_{12}}{E_1} - \frac{1}{G_{12}}\right)\sin\theta\cos^3\theta - \left(\frac{2}{E_2} + \frac{2\nu_{12}}{E_1} - \frac{1}{G_{12}}\right)\sin^3\theta\cos\theta\right] \tag{23}$$

$$\eta_{xy,y} = E_y\left[\left(\frac{2}{E_1} + \frac{2\nu_{12}}{E_1} - \frac{1}{G_{12}}\right)\sin^3\theta\cos\theta - \left(\frac{2}{E_2} + \frac{2\nu_{12}}{E_1} - \frac{1}{G_{12}}\right)\sin\theta\cos^3\theta\right] \tag{24}$$

The $\eta_{ij,i}$ terms are called the coefficient of mutual influence, which characterizes shearing in the *ij*-plane caused by a normal stress in the *i*-direction.

In order to derive the expressions used for the strains, certain assumptions are made. Consider a laminated plate consisting of a number of fiber-reinforced laminae. Let u, v, w be the displacement components in x, y, z directions, respectively, as depicted in figure 42, and the x-y plane is located at the mid-plane of the plate where z is the direction of the normal to the middle surface. Since the thicknesses of laminated plates of practical interest are usually small as compared with the lateral dimensions, it is assumed that the variation over the thickness is small. Also, assume that the deformed mid-plane remains perpendicular to the plane section when the laminate is extended or bent. Then the strains are given by

$$\begin{aligned} \varepsilon_{xx} &= \varepsilon_x^o + z\kappa_x \\ \varepsilon_{yy} &= \varepsilon_y^o + z\kappa_y \\ \gamma_{xy} &= \gamma_{xy}^o + z\kappa_{xy} \end{aligned} \tag{25}$$

where

$$\varepsilon_x^o = \frac{\partial u_o}{\partial x}, \quad \varepsilon_y^o = \frac{\partial v_o}{\partial y}, \quad \gamma_{xy}^o = \frac{\partial u_o}{\partial y} + \frac{\partial u_o}{\partial x} \tag{26}$$

$$\kappa_x = -\frac{\partial^2 w_o}{\partial x^2}, \quad \kappa_y = -\frac{\partial^2 w_o}{\partial y^2}, \quad \kappa_{xy} = -2\frac{\partial^2 w_o}{\partial x \partial y} \tag{27}$$

Thus, the strains of the laminate are continuous over the thickness, and are described by the middle surface strains ε_x^o, ε_y^o, γ_{xy}^o, and the middle surface curvatures, κ_x, κ_y, κ_{xy}.

In order to derive the plates constitutive equations, consider the kth layer of a multilayered laminate. Then for the kth layer, the stress components are given by

$$\begin{Bmatrix}\sigma_{xx}\\ \sigma_{yy}\\ \sigma_{xy}\end{Bmatrix}_k = \begin{bmatrix}\overline{Q}_{11} & \overline{Q}_{12} & \overline{Q}_{16}\\ \overline{Q}_{12} & \overline{Q}_{22} & \overline{Q}_{26}\\ \overline{Q}_{16} & \overline{Q}_{26} & \overline{Q}_{66}\end{bmatrix}_k \left(\begin{Bmatrix}\varepsilon_x^o\\ \varepsilon_y^o\\ \gamma_{xy}^o\end{Bmatrix} + z\begin{Bmatrix}\kappa_x\\ \kappa_y\\ \kappa_{xy}\end{Bmatrix} \right) \tag{28}$$

The resultant forces {N} and moments {M} acting on a laminate are obtained by integration of the stresses in each layer through the laminate thickness, h, and are given by

$$\begin{Bmatrix}N_x\\ N_y\\ N_{xy}\end{Bmatrix} = \int_{-h/2}^{h/2} \begin{Bmatrix}\sigma_{xx}\\ \sigma_{yy}\\ \sigma_{xy}\end{Bmatrix} dz \quad \text{and} \quad \begin{Bmatrix}M_x\\ M_y\\ M_{xy}\end{Bmatrix} = \int_{-h/2}^{h/2} \begin{Bmatrix}\sigma_{xx}\\ \sigma_{yy}\\ \sigma_{xy}\end{Bmatrix} z dz \tag{29}$$

where h denotes the thickness of the plate. For a laminate with n layers, the integrals in equation (29) can be expressed as

$$\begin{Bmatrix}N_x\\ N_y\\ N_{xy}\end{Bmatrix} = \sum_{k=1}^{n} \int_{z_{k-1}}^{z_k} \begin{Bmatrix}\sigma_{xx}\\ \sigma_{yy}\\ \sigma_{xy}\end{Bmatrix}_k dz \quad \text{and} \quad \begin{Bmatrix}M_x\\ M_y\\ M_{xy}\end{Bmatrix} = \sum_{k=1}^{n} \int_{z_{k-1}}^{z_k} \begin{Bmatrix}\sigma_{xx}\\ \sigma_{yy}\\ \sigma_{xy}\end{Bmatrix}_k z dz \tag{30}$$

Substituting (28) into (30), we obtain

$$\begin{Bmatrix}N_x\\ N_y\\ N_{xy}\end{Bmatrix} = \sum_{k=1}^{n} \left[\overline{Q}\right]_k \left(\int_{z_{k-1}}^{z_k} \begin{Bmatrix}\varepsilon_x^o\\ \varepsilon_y^o\\ \gamma_{xy}^o\end{Bmatrix} dz + \int_{z_{k-1}}^{z_k} \begin{Bmatrix}\kappa_x\\ \kappa_y\\ \kappa_{xy}\end{Bmatrix} z dz \right) \tag{31}$$

and

$$\begin{Bmatrix} M_x \\ M_y \\ M_{xy} \end{Bmatrix} = \sum_{k=1}^{n} \left[\overline{Q}\right]_k \left(\int_{z_{k-1}}^{z_k} \begin{Bmatrix} \varepsilon_x^o \\ \varepsilon_y^o \\ \gamma_{xy}^o \end{Bmatrix} z dz + \int_{z_{k-1}}^{z_k} \begin{Bmatrix} \kappa_x \\ \kappa_y \\ \kappa_{xy} \end{Bmatrix} z^2 dz \right) \tag{32}$$

Note that the quantities $\varepsilon_x^o, \varepsilon_y^o, \kappa_x, \kappa_y, \kappa_{xy}$ are independent of z. Thus, the integrations in (31) and (32) can be easily performed. The combined results can be expressed in the following form:

$$\left\{\begin{array}{c} N_x \\ N_y \\ N_{xy} \\ \hline M_x \\ M_y \\ M_{xy} \end{array}\right\} = \left[\begin{array}{ccc:ccc} A_{11} & A_{12} & A_{16} & B_{11} & B_{12} & B_{16} \\ A_{12} & A_{22} & A_{26} & B_{12} & B_{22} & B_{26} \\ A_{16} & A_{26} & A_{66} & B_{16} & B_{26} & B_{66} \\ \hdashline B_{11} & B_{12} & B_{16} & D_{11} & D_{12} & D_{16} \\ B_{12} & B_{22} & B_{26} & D_{12} & D_{11} & D_{26} \\ B_{16} & B_{26} & B_{66} & D_{16} & D_{26} & D_{66} \end{array}\right] \left\{\begin{array}{c} \varepsilon_x^o \\ \varepsilon_y^o \\ \gamma_{xy}^o \\ \hline \kappa_x \\ \kappa_y \\ \kappa_{xy} \end{array}\right\} \tag{33}$$

where

$$(A_{ij}, B_{ij}, D_{ij}) = \int_{-h/2}^{h/2} \overline{Q}_{ij}^{(k)} (1, z, z^2) dz \tag{34}$$

Or, explicitly,

$$A_{ij} = \sum_{k=1}^{n} \overline{Q}_{ij}^{(k)} (z_k - z_{z-1})$$

$$B_{ij} = \frac{1}{2} \sum_{k=1}^{n} \overline{Q}_{ij}^{(k)} (z_k^2 - z_{k-1}^2) \tag{35}$$

$$D_{ij} = \frac{1}{3} \sum_{k=1}^{n} \overline{Q}_{ij}^{(k)} (z_k^3 - z_{k-1}^3)$$

Denoting the thickness and the distance to the centroid of the kth layer by t_k and $\bar{z}_k$, respectively, we can also write (35) as

$$A_{ij} = \sum_{k=1}^{n} \overline{Q}_{ij}^{(k)} t_k$$

$$B_{ij} = \sum_{k=1}^{n} \overline{Q}_{ij}^{(k)} t_k \bar{z}_k \tag{36}$$

$$D_{ij} = \sum_{k=1}^{n} \overline{Q}_{ij}^{(k)} \left(t_k \bar{z}_k^2 + \frac{t_k^3}{12} \right)$$

Coefficients A_{ij} are called extensional stiffness, B_{ij} are the coupling stiffnesses, and D_{ij} are the bending stiffnesses.

Symbolically, (33) is usually expressed in the form

$$\begin{Bmatrix} N \\ \hline M \end{Bmatrix} = \left[\begin{array}{c|c} A & B \\ \hline B & D \end{array}\right] \begin{Bmatrix} \varepsilon^o \\ \hline \kappa \end{Bmatrix} \tag{37}$$

9.2 Thermal Stresses

In unidirectional fiber composites, the thermal expansion is orthotropic. The linear thermal expansion coefficients in the fiber direction and the transverse direction are denoted as α_1 and α_2, respectively. The units of α are strain per degree of temperature. The thermal strains (ε^T) induced by a temperature change ΔT are given by

$$\begin{Bmatrix} \varepsilon_{11}^T \\ \varepsilon_{22}^T \\ \gamma_{12}^T \end{Bmatrix} = \begin{Bmatrix} \alpha_1 \\ \alpha_2 \\ 0 \end{Bmatrix} \Delta T \tag{38}$$

The stress-strain relations for a plane stress unidirectional fiber composite are modified to

$$\{\sigma\} = [Q]\left(\{\varepsilon\} - \{\varepsilon^T\}\right) \tag{39}$$

in reference to the material principal axes.

Looking at equation (38), the thermal expansion coefficients $\{\alpha\}$ should transform identically as the strains. That is,

$$\begin{Bmatrix} \alpha_1 \\ \alpha_2 \\ 0 \end{Bmatrix} = [T_\varepsilon] \begin{Bmatrix} \alpha_x \\ \alpha_y \\ \alpha_{xy} \end{Bmatrix} \tag{40}$$

The inverse of the relationship (40) can be readily obtained as

$$\begin{aligned} \alpha_x &= \alpha_1 \cos^2\theta + \alpha_2 \sin^2\theta \\ \alpha_y &= \alpha_1 \sin^2\theta + \alpha_2 \cos^2\theta \\ \alpha_{xy} &= 2(\alpha_1 - \alpha_2)\sin\theta\cos\theta \end{aligned} \tag{41}$$

Using the Kirchhoff assumptions given by (25), the relation (39) in the global coordinate x-y system can be written as

$$\begin{Bmatrix} \sigma_{xx} \\ \sigma_{yy} \\ \sigma_{xy} \end{Bmatrix} = \begin{bmatrix} \overline{Q}_{11} & \overline{Q}_{12} & \overline{Q}_{16} \\ \overline{Q}_{12} & \overline{Q}_{22} & \overline{Q}_{26} \\ \overline{Q}_{16} & \overline{Q}_{26} & \overline{Q}_{66} \end{bmatrix} \left(\begin{Bmatrix} \varepsilon_x^o \\ \varepsilon_y^o \\ \gamma_{xy}^o \end{Bmatrix} + z \begin{Bmatrix} \kappa_x \\ \kappa_y \\ \kappa_{xy} \end{Bmatrix} - \begin{Bmatrix} \alpha_x \Delta T \\ \alpha_y \Delta T \\ \alpha_{xy} \Delta T \end{Bmatrix} \right) \tag{42}$$

Following the procedure that was used in plate theory to obtain equation (37), we obtain the plate constitutive equation as

$$\begin{Bmatrix} N \\ \hline M \end{Bmatrix} = \begin{bmatrix} A & B \\ \hline B & D \end{bmatrix} \begin{Bmatrix} \varepsilon^o \\ \hline \kappa \end{Bmatrix} - \begin{Bmatrix} N^T \\ \hline M^T \end{Bmatrix} \tag{43}$$

where

$$\left\{N^T\right\} \begin{Bmatrix} N_x^T \\ N_y^T \\ N_{xy}^T \end{Bmatrix} = \int_{-h/2}^{h/2} \left[\overline{Q}\right] \begin{Bmatrix} \alpha_x \\ \alpha_y \\ \alpha_{xy} \end{Bmatrix} \Delta T dz \tag{44}$$

$$\left\{M^T\right\} \begin{Bmatrix} M_x^T \\ M_y^T \\ M_{xy}^T \end{Bmatrix} = \int_{-h/2}^{h/2} \left[\overline{Q}\right] \begin{Bmatrix} \alpha_x \\ \alpha_y \\ \alpha_{xy} \end{Bmatrix} \Delta T z dz \tag{45}$$

After integration over the laminae, the expressions in (44) and (45) can be written explicitly as

$$\left\{N^T\right\} = \Delta T \sum_{k=1}^{n} \overline{Q}^{(k)} \{\alpha\}_k \, t_k$$

$$\left\{M^T\right\} = \frac{1}{2} \Delta T \sum_{k=1}^{n} \overline{Q}^{(k)} \{\alpha\}_k \left(z_k^2 - z_{k-1}^2\right) \tag{46}$$

9.3 Calculated Transverse Ply Stress

As shown by many of the studies cited in the Introduction section, in the absence of mechanical loading, thermal stresses alone may be sufficient to influence laminate performance. For thermal loading, stresses are induced at the ply level due to expansion or contraction and constraining effects of adjacent plies that prevent a free expansion or contraction. The residual stress in any ply can be calculated using classical laminated plate theory as discussed in the section 9.1. In general, for a laminated, unidirectional plate under plane stress, the constitutive relationship given by equation (39) includes the combination of the total and thermal strains where σ is the

stress, Q is the material stiffness matrix, ε is the total strain and ε^T is the thermal strain. Also, recall that for a single lamina or ply, the thermal strain is calculated using equation (38), where ε is the normal strain, γ is the shear strain, α is the coefficient of thermal expansion (CTE), and ΔT is the temperature differential between the test condition and the stress free condition at cure. Subscripts in equation (38) refer to the standard notation (1 = fiber direction, 2 = transverse direction). Clearly, from equation (38) it is apparent that for large values of ΔT, a condition at cryogenic temperatures, the magnitude of the thermal induced strains is highly dependent on the material CTE values. In particular, nonlinear behavior of the CTE with respect to temperature, as illustrated in table 6, may result in thermal residual stresses that also vary in a nonlinear manner with respect to temperature. To illustrate this effect, material tensile properties given in table 2 and CTE values derived from [17] (provided in table 6) were used as inputs to classical laminated plate theory to predict the maximum transverse ply stress as a function of laminate stacking sequence, test temperature, and laminate preconditioning. For example, to obtain the ply stresses for a laminate at –196°C, and aged without load, the values from table 2 that were used as input included E_1 = 146.3 GPa, E_2 = 9.5 GPa, and G_{12} = 6.2 GPa. The CTE values at –196°C used from table 6 included α_1 = –1.49 μmm/mm-°C and α_2 = 20.5 μmm/mm-°C. The results of these calculations are given in table 7. It should be noted that not-aged CTE values were used for all conditions and the stress-free temperature was assumed to be the glass transition temperature of IM7/PETI-5. With respect to temperature, table 7 indicates that the trend for the not-aged condition is for transverse stress to increase with a decrease in temperature. However, both of the isothermal-aged conditions predict the largest stress to occur at the intermediate temperature (–196°C), as shown in the plots of the maximum transverse ply stress as a function of temperature (figure 43). With respect to ply lay-up, the highly constrained $[45/90_3/\text{-}45/\bar{0}_3]_S$ –ply laminate is predicted to have the highest stress at any given temperature, however the angle-ply laminate $[\pm 45]_{3S}$ –ply laminate has stress magnitudes close to the $[45/90_3/\text{-}45/\bar{0}_3]_S$ –ply laminate. Since the measured tensile strength (58 MPa) at –196°C of the aged-without-load $[90]_{12}$ –ply laminate was less than the calculated transverse ply stress (88.3 MPa) at –196°C in the aged-without-load $[45/90_3/\text{-}45/\bar{0}_3]_S$ –ply laminate, it was expected that matrix

cracking would have occurred after aging. Even though surface degradation was apparent, no matrix cracks were observed, indicating that the ply stresses were not high enough to cause matrix cracking.

Transverse ply stresses may be of more interest in a tensile loading mode due to the fact that matrix cracking, caused by residual stresses, is a more prevalent damage mechanism in tension than in compression. Nevertheless, for the sake of comparison, the compressive material properties given in table 3 were also used as inputs to classical laminated plate theory to predict the maximum transverse ply stress as a function of laminate stacking sequence, test temperature, and laminate preconditioning. These results are given in table 8. The stresses increase as temperature decreases with little difference due to aging either with or without load as shown in figure 44. Here again, the $[45/90_3/-45/\bar{0}_3]_S$ –ply laminate showed higher stress than the $[\pm 25]_{3S}$ –ply laminate, and only slightly higher than the $[\pm 45]_{3S}$ –ply laminate.

10. SUMMARY AND CONCLUDING REMARKS

Five different laminate configurations of IM7/PETI-5 were evaluated for tensile and compressive strength and stiffness at room temperature and two cryogenic test temperatures. The effects of laminate configuration, test temperature, and preconditioning or aging were investigated. Aging consisted of 576 hours exposure in a –184°C environment both with and without mechanical load. Specimens were also examined for evidence of damage or microcracking before and after aging. The fracture surfaces were examined for distinguishing features that could be attributed to test temperature or aging conditions. Classical Lamination Theory was used to calculate the transverse ply stresses due to thermal loading.

Examination of the basic lamina properties such as strength and stiffness in the longitudinal, transverse, and shear directions indicates that cryogenic temperatures can have an appreciable influence on behavior. In tension, longitudinal and transverse stiffness and strength will decrease as the test temperature is decreased. The tensile shear modulus and strength will

increase as the temperature is decreased. In tension, the lamination stacking sequences such as the $[45/90_3/-45/\bar{0}_3]_S$ and $[\pm 25]_{3S}$ are less influenced by temperature, however the highly constrained $[45/90_3/-45/\bar{0}_3]_S$–ply laminate is more sensitive to cryogenic temperatures than the $[\pm 25]_{3S}$–ply laminate. In compression, cryogenic temperatures will produce an increase in both the modulus and strength of all the laminates. The greatest increase in compressive strength occurs in the $[90]_{12}$–ply laminates and the greatest increase in modulus occurs in the $[\pm 45]_{3S}$–ply laminates.

Aging the material under isothermal, cryogenic temperature caused changes in the strength and stiffness as compared to the not aged or as-received condition. In general, it appears that this type of aging increased both tensile strength and stiffness, particularly in the $[\pm 45]_{3S}$, $[90]_{12}$, and the $[45/90_3/-45/\bar{0}_3]_S$–ply laminates. Of particular interest, isothermal cryogenic aging while under a constant strain condition produced some additional increase in tensile strength and stiffness as compared to aging in an unloaded condition of the $[45/90_3/-45/\bar{0}_3]_S$–ply laminates. The aging tends to decrease the compressive strength and stiffness in the $[\pm 45]_{3S}$, $[90]_{12}$, and the $[0]_{12}$ –ply laminates.

Aging did not change the fracture surface characteristics in either tension or compression. Dissimilarities occurred in the tensile specimen fractures due to testing in cryogenic fluids as opposed to the room temperature tests. In general, the fracture surfaces from the room temperature tests appeared catastrophic having irregular breaks whereas the specimens tested at cryogenic temperatures exhibited clean breaks of a more regular appearance. This was attributed to the ductility of the matrix material at room temperature verses the brittle nature of the matrix at low temperatures.

For the IM7/PETI-5 material, aging at cryogenic temperatures also produced degradation in the matrix material along the exposed edges. This degradation may have had an adverse influence on residual strength due to the increase in possible failure initiation sites.

Residual stress calculations based on lamination theory showed that the transverse ply stresses are high for cryogenic test temperatures. The transverse ply stresses calculated using the tensile moduli values as input indicate that the highest stresses occur at the intermediate test temperature of –196°C in the aged materials, with and without load. The residual stress values calculated using the compressive moduli values indicate an increasing transverse ply stress as temperature decreases with the not aged material producing slightly higher stresses than the aged material. These transverse residual stresses may lower potential strength and stiffness by accelerating the initiation and growth of transverse microcracks in a ply.

It is apparent from the material properties generated and the ply stress analysis, it cannot be assumed that the lowest test temperatures are necessarily the worst case. It has been shown in several cases, especially the tensile strength, that the lowest strength occurs at –196°C. The tensile ply stress analysis supports this finding by predicting the highest transverse ply stresses to be at –196°C in the aged material.

It should be recognized that there is a difference between tension and compression results. Experimental test matrices should not be limited to one mode or the other, and expect to infer conclusions about the other failure mode.

11. FUTURE RESEARCH

One of the questions left unanswered by this study is, "What is damage as a function of aging time?" The aging process used is this study was an arbitrarily determined aging time and temperature of 576 hours at –184°C. Future studies may include longer aging times to determine the time-dependent function of residual stress development. Strain levels chosen for the pre-aging conditions defined in this study may not have been high enough to produce sufficient findings on the effects of aging with load. It would be of interest to conduct further aging with various static loads. Because cryogenics tanks may be subjected to extreme thermal difference,

thermal cycling studies down to –269°C from some elevated temperature should be investigated. Because the IM7/PETI-5 material did not show microcrack damage from the aging conditions it was subjected to for this thesis, it may be a suitable candidate material for permeability studies.

12. REFERENCES

1. O'Brien, T.K., "Fracture Mechanics of Composite Delamination," *ASM Handbook, Composites*, ASM International, Vol. 21 2001,. pp. 241-245.

2. Timmerman, J.F., et al., "Matrix and fiber influences on the cryogenic microcracking of carbon fiber/epoxy composites" *Composites Part A: Applied Science and manufacturing*, Vol. 33, 2002, pp. 323-329.

3. Robinson, M.J., "Composite Structures on the DC-XA Reusable Launch Vehicle," 28th International SAMPE, Seattle, Washington, 1996.

4. Robinson, M.J., "Composite Cryogenic Propellant Tank Development," 35th Structures, Structural Dynamics, and Materials Conference, Hilton Head, South Carolina, 1994.

5. Callaghan, M.T., "Use of resin composites for cryogenic tankage," *Cryogenics*, Vol. 31, No. 4, 1991, pp. 282-287.

6. Morino, Y., et al. "Feasibility Study of CFRP Material Application to the Cryogenic Propellant Tank of Reusable Launch Vehicles," 6th Japan International SAMPE Symposium, Japan 1999.

7. Pannkoke, K. and Wagner, H.J., "Fatigue properties of unidirectional carbon fiber composites at cryogenic temperatures," *Cryogenics*, Vol. 31, No. 4, 1991, pp. 248-251.

8. Ahlborn, K., "Cryogenic mechanical response of carbon fibre reinforced plastics with thermoplastic matrices to quasi-static loads," *Cryogenics*, Vol. 31, No. 4, 1991, pp. 252-256.

9. Ahlborn, K.,"Durability of carbon fibre reinforced plastics with thermoplastic matrices under cyclic mechanical and cyclic thermal loads at cryogenic temperatures," *Cryogenics*, Vol. 31, No. 4, 1991, pp. 257-260.

10. Perepechko, I., *Low-Temperature Properties of Polymers*, Mir Publishers, Moscow, 1997.

11. Schutz, J.B., "Properties of composite materials for cryogenic applications," *Cryogenics*, Vol. 38, No. 1, 1998, pp. 3-12.

12. Schoeppner, G.A., Kim, R. and Donaldson, S.L., "Steady State Cracking of PMC's at Cryogenic Temperatures," AIAA 42nd SDM Conference, Seattle, WA, 2001.

13. Kampf, G., *Characterization of Plastics by Physical Methods, Experimental Techniques, and Practical Application*, Munic, Hanser, 1986.

14. Council, N.R., ed. *U.S. Supersonic Commercial Aircraft*. Committee on High Speed Research Aeronautics and Space Engineering Board, National Academy Press, Washington, D.C., 1997.

15. Dally, J.W. and Riley, W.F. *Experimental Stress Analysis*. 2 ed., McGraw-Hill Book Company, New York, 1978.

16. Jones, R.M., *Mechanics of Composite Materials*, Washington, D.C., Scripta Book Company, 1975.

17. Johnson, T.F. and Gates, T.S., "High Temperature Polyimide Materials in Extreme Temperature Environments," 42nd AIAA/ASME/ASCE/AHS/ASC Structural Dynamics, and Materials Conference, Seattle, WA. 2001.

Table 1. Test matrix including the residual test temperature and aging condition for each type of laminate lay-up.

Test Temp (°C)	Aging Condition (–184°C)		
	No Load	Static Load (3000 με)	Static Load (4000 με)
23	$[0]_{12}$, $[90]_{12}$, $[\pm45]_{3S}$, $[\pm25]_{3S}$, $[45/90_3/-45/\overline{0}_3]_S$	$[\pm45]_{12}$, $[0]_{12}$	$[\pm25]_{3S}$, $[45/90_3/-45/\overline{0}_3]_S$
–196	$[0]_{12}$, $[90]_{12}$, $[\pm45]_{3S}$, $[\pm25]_{3S}$, $[45/90_3/-45/\overline{0}_3]_S$	$[\pm45]_{12}$, $[0]_{12}$	$[\pm25]_{3S}$, $[45/90_3/-45/\overline{0}_3]_S$
–269	$[0]_{12}$, $[90]_{12}$, $[\pm45]_{3S}$, $[\pm25]_{3S}$, $[45/90_3/-45/\overline{0}_3]_S$	$[\pm45]_{12}$, $[0]_{12}$	$[\pm25]_{3S}$, $[45/90_3/-45/\overline{0}_3]_S$

Table 2. Measured tensile elastic modulus values

Specimen ply lay - up	Temp °C	Material property	Not aged modulus (GPa) ± Std dev.	Aged without load modulus (GPa) ± Std dev.	Aged with load modulus (GPa) ± Std dev.
$[0]_{12}$	24	E_1	157.6 ± 9.3	153.6 ± 5.9	147.2 ± 2.6
$[0]_{12}$	-196	E_1	151.6 ± 2.2	146.3 ± 11.5	149.2 ± 1.9
$[0]_{12}$	-269	E_1	145.1 ± 7.4	143.0 ± 8.8	158.6 ± 20.8
$[\pm 25]_{3S}$	24	E_x	71.9 ± 1.0	70.3 ± 1.6	59.8 ± 2.6
$[\pm 25]_{3S}$	-196	E_x	75.7 ± 0.8	63.8 ± 8.5	71.5 ± 3.0
$[\pm 25]_{3S}$	-269	E_x	73.1 ± 3.7	69.4	65.6 ± 12.2
$[45/90_3/-45/\bar{0}_3]_S$	24	E_x	50.7 ± 1.0	46.7 ± 4.3	51.0 ± 1.1
$[45/90_3/-45/\bar{0}_3]_S$	-196	E_x	40.6 ± 5.9	48.0 ± 1.8	48.6 ± 3.0
$[45/90_3/-45/\bar{0}_3]_S$	-269	E_x	43.8 ± 1.9	44.3 ± 3.9	52.1 ± 1.3
$[90]_{12}$	24	E_2	8.7 ± 0.1	8.6 ± 0.1	NA
$[90]_{12}$	-196	E_2	7.5 ± 0.1	9.5 ± 2.0	9.6 ± 0.1
$[90]_{12}$	-269	E_2	7.8 ± 1.2	7.1 ± 0.8	NA
$[\pm 45]_{3S}$	24	G_{12}	4.6 ± 0.4	5.0 ± 0.1	5.8 ± 0.2
$[\pm 45]_{3S}$	-196	G_{12}	5.8 ± 0.1	6.2 ± 0.1	6.0 ± 0.2
$[\pm 45]_{3S}$	-269	G_{12}	6.2 ± 0.2	5.5 ± 0.9	6.1 ± 0.3

(NA = not available)

Table 3. Measured compressive elastic modulus values

Specimen ply lay - up	Temp °C	Material property	Not aged modulus (GPa) ± Std dev.	Aged without load modulus (GPa) ± Std dev.	Aged with load modulus (GPa) ± Std dev.
$[0]_{12}$	24	E_1	135.2 ± 1.1	139.0 ± 3	129.9 ± 4.8
$[0]_{12}$	-196	E_1	142.0 ± 15.0	154.0 ± 5.9	147.9 ± 5.5
$[0]_{12}$	-269	E_1	146.9 ± 11.1	143.1 ± 6.0	139.9 ± 11.4
$[\pm 25]_{3S}$	24	E_x	63.2 ± 5.7	60.0 ± 4.1	62.8 ± 3.1
$[\pm 25]_{3S}$	-196	E_x	64.1 ± 7.5	72.1 ± 8.0	72.6 ± 2.5
$[\pm 25]_{3S}$	-269	E_x	77.5 ± 17.5	77.3 ± 9.4	69.5 ± 1.7
$[45/90_3/-45/\bar{0}_3]_S$	24	E_x	44.3 ± 5.1	46.3 ± 0.9	40.7 ± 7.6
$[45/90_3/-45/\bar{0}_3]_S$	-196	E_x	60.6 ± 7.3	50.8 ± 4.8	52.2 ± 7.0
$[45/90_3/-45/\bar{0}_3]_S$	-269	E_x	51.2 ± 4.2	47.6 ± 1.1	53.7 ± 5.0
$[90]_{12}$	24	E_2	11.6 ± 1.7	12.1 ± 0.5	NA
$[90]_{12}$	-196	E_2	11.9 ± 1.1	11.1 ± 0.5	NA
$[90]_{12}$	-269	E_2	12.8 ± 1.1	12.2 ± 01.6	NA
$[\pm 45]_{3S}$	24	G_{12}	4.8 ± 2.5	5.3 ± 0.5	4.3 ± 0.1
$[\pm 45]_{3S}$	-196	G_{12}	6.7 ± 0.8	5.4 ± 0.5	6.0 ± 1.2
$[\pm 45]_{3S}$	-269	G_{12}	7.6 ± 3.0	5.8 ± 0.3	7.0 ± 2.0

(NA = not available)

Table 4. Measured tensile strength values

Specimen ply lay- up	Temp °C	Not aged strength (MPa) ± Std dev.	Aged without load strength (MPa) ± Std dev.	Aged with load strength (MPa) ± Std dev.
$[0]_{12}$	24	1940 ± 276	1865 ± 44	1848 ± 49
$[0]_{12}$	-196	1287 ± 207	1568 ± 59	1536 ± 126
$[0]_{12}$	-269	1495 ± 326	1451 ± 243	1771 ± 186
$[\pm 25]_{3S}$	24	1132 ± 77	1266 ± 58	955 ± 84
$[\pm 25]_{3S}$	-196	912 ± 49	902 ± 208	1120 ± 51
$[\pm 25]_{3S}$	-269	1131 ± 15	1114	1024 ± 209
$[45/90_3/-45/\bar{0}_3]_S$	24	711 ± 14	700 ± 67	843 ± 38
$[45/90_3/-45/\bar{0}_3]_S$	-196	585 ± 119	748 ± 57	872 ± 40
$[45/90_3/-45/\bar{0}_3]_S$	-269	656 ± 48	732 ± 64	806 ± 2
$[90]_{12}$	24	47 ± 2	47 ± 3	NA
$[90]_{12}$	-196	21 ± 4	58 ± 30	63 ± 5
$[90]_{12}$	-269	17 ± 4	11 ± 5	NA
$[\pm 45]_{3S}$	24	163 ± 2	165 ± 1	182 ± 4
$[\pm 45]_{3S}$	-196	242 ± 4	249 ± 3	245 ± 8
$[\pm 45]_{3S}$	-269	256 ± 8	257 ± 12	257 ± 5

(NA = not available) Note: Tensile strength of $[\pm 45]_{3S}$ was defined as the initial point of deviation from the tangent of the nearly horizontal slope of the stress strain curve.

Table 5. Measured compressive strength values

Specimen ply lay- up	Temp °C	Not aged strength (MPa) ± Std dev.	Aged without load strength (MPa) ± Std dev.	Aged with load strength (MPa) ± Std dev.
$[0]_{12}$	24	857.5 ± 52.5	856.2 ± 102.4	817.4 ± 74.2
$[0]_{12}$	-196	1124.8 ± 127.6	1167.2 ± 60.9	1115.2 ± 66.2
$[0]_{12}$	-269	1193.5 ± 100.8	1234.7 ± 44.6	1156.1 ± 61.0
$[\pm 25]_{3S}$	24	502.9 ± 65.7	467.7 ± 37.2	524.8 ± 43.4
$[\pm 25]_{3S}$	-196	604.2 ± 9.6	709.5 ± 0.3	685.6 ± 87.2
$[\pm 25]_{3S}$	-269	714.8 ± 132.7	749.4 ± 27.2	571.2 ± 61.5
$[45/90_3/-45/\bar{0}_3]_S$	24	473.3 ± 121.8	432.6 ± 10.2	530.6 ± 107.5
$[45/90_3/-45/\bar{0}_3]_S$	-196	375.7 ± 130.1	554.3 ± 29.8	709.5 ± 89.2
$[45/90_3/-45/\bar{0}_3]_S$	-269	572.2 ± 28.6	619.1 ± 11.9	723.0 ± 113.4
$[90]_{12}$	24	220.0 ± 10.0	280.0 ± 11.5	NA
$[90]_{12}$	-196	293.7 ± 16.1	273.7 ± 52.7	NA
$[90]_{12}$	-269	367.6 ± 35.1	301.9 ± 21.8	NA
$[\pm 45]_{3S}$	24	426.7 ± 27.7	398.3 ± 26.4	364.8 ± 12.2
$[\pm 45]_{3S}$	-196	536.8 ± 73.3	511.0 ± 57.1	530.5 ± 21.4
$[\pm 45]_{3S}$	-269	578.1 ± 13.8	569.5 ± 10.38	454.6 ± 98.0

(NA = not available)

Table 6. Coefficient of thermal expansion for not aged IM7/PETI-5 material system

Temp (°C)	μ mm/mm – °C	
	α_1	α_2
24	–1.30	19.45
–196	–1.49	20.05
–273	–2.77	18.46

Table 7. Calculated maximum transverse ply stress for thermal loading only, using tensile modulus values.

Precondition	Temp (°C)	Maximum transverse ply stress, σ_{22} (MPa)			
		$[0]_{12}$	$[\pm 25]_{3S}$	$[45/90_3/-45/\bar{0}_3]_S$	$[\pm 45]_{3S}$
Not aged	24	0.0	18.2	41.3	40.6
	–196	0.0	37.7	70.9	69.7
	–269	0.0	45.7	83.7	82.3
Iso-aged without load	24	0.0	18.9	40.8	40.1
	–196	0.0	43.6	88.3	86.5
	–269	0.0	40.8	76.5	75.3
Iso-aged with load	24	0.0	20.4	40.7	39.9
	–196	0.0	43.1	89.3	87.5
	–269	0.0	42.9	76.9	75.8

Table 8. Calculated maximum transverse ply stress for thermal loading only, using compressive modulus values.

Precondition	Temp (°C)	Maximum transverse ply stress (MPa)			
		$[0]_{12}$	$[\pm 25]_{3S}$	$[45/90_3/-45/\bar{0}_3]_S$	$[\pm 45]_{3S}$
Not aged	24	0.0	20.7	53.4	51.9
	–196	0.0	50.0	108.6	105.6
	–269	0.0	62.9	132.8	129.1
Iso-aged without load	24	0.0	22.3	55.7	54.1
	–196	0.0	43.4	102.5	100.1
	–269	0.0	53.3	126.9	123.3
Iso-aged with load	24	0.0	19.6	55.4	53.7
	–196	0.0	45.9	102.2	99.7
	–269	0.0	58.9	126.6	123.0

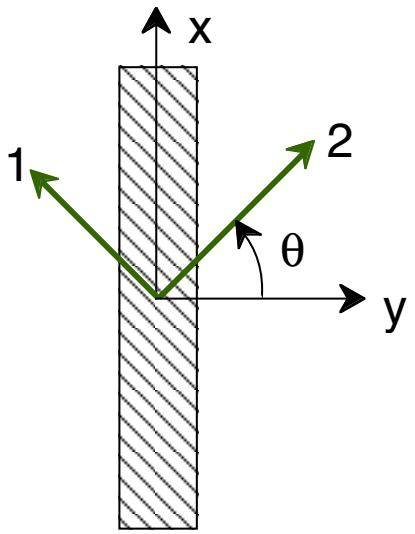

Figure 1. Schematic of coordinate axes for a unidirectional composite. Axis-1 is along the fiber direction, and axis-2 is transverse to the fiber. The x-y axes are fixed to the body coordinate.

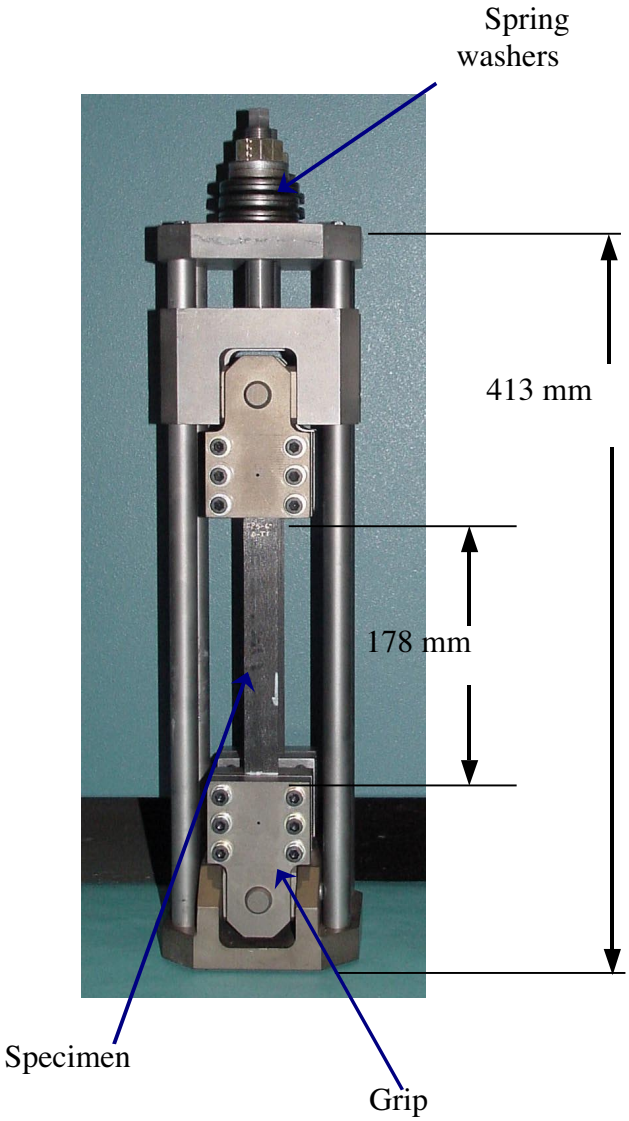

Figure 2. Constant strain fixture.

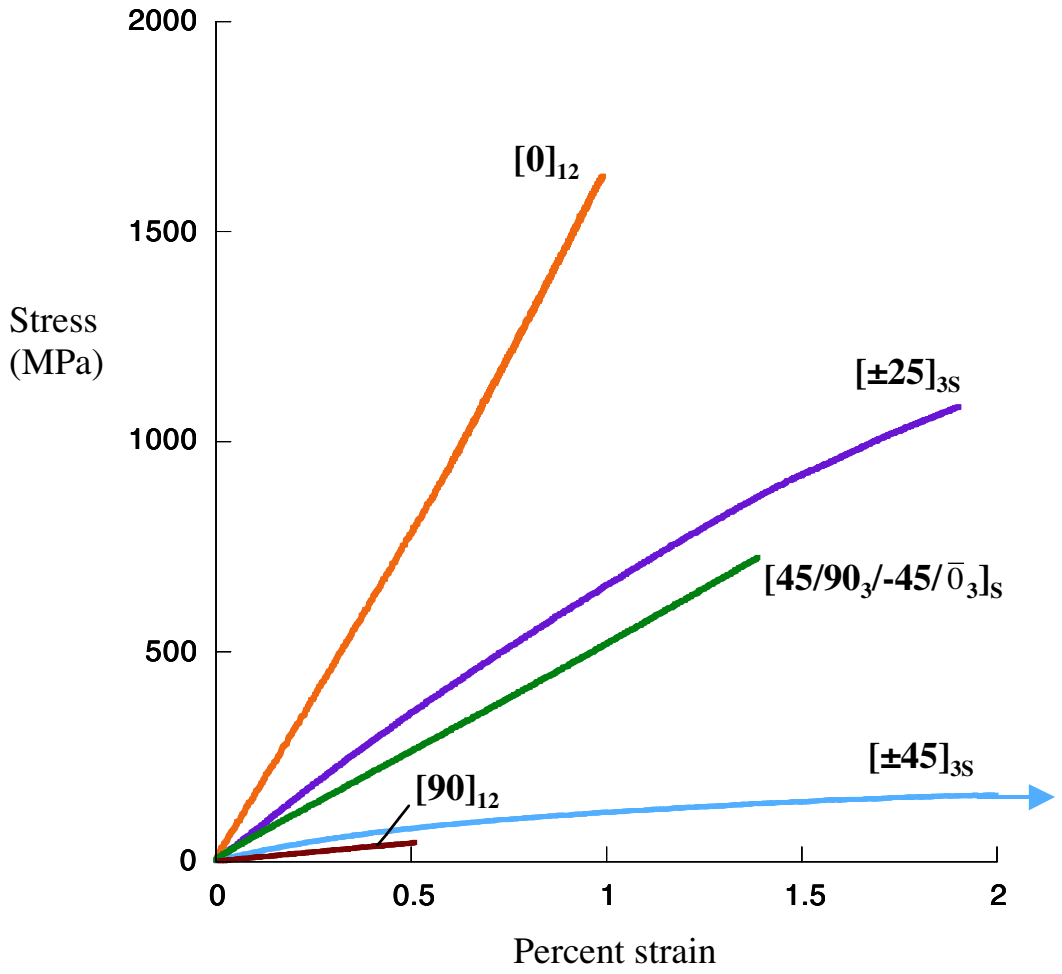

Figure 3. Room temperature stress-strain curves of 5 the lay-ups.

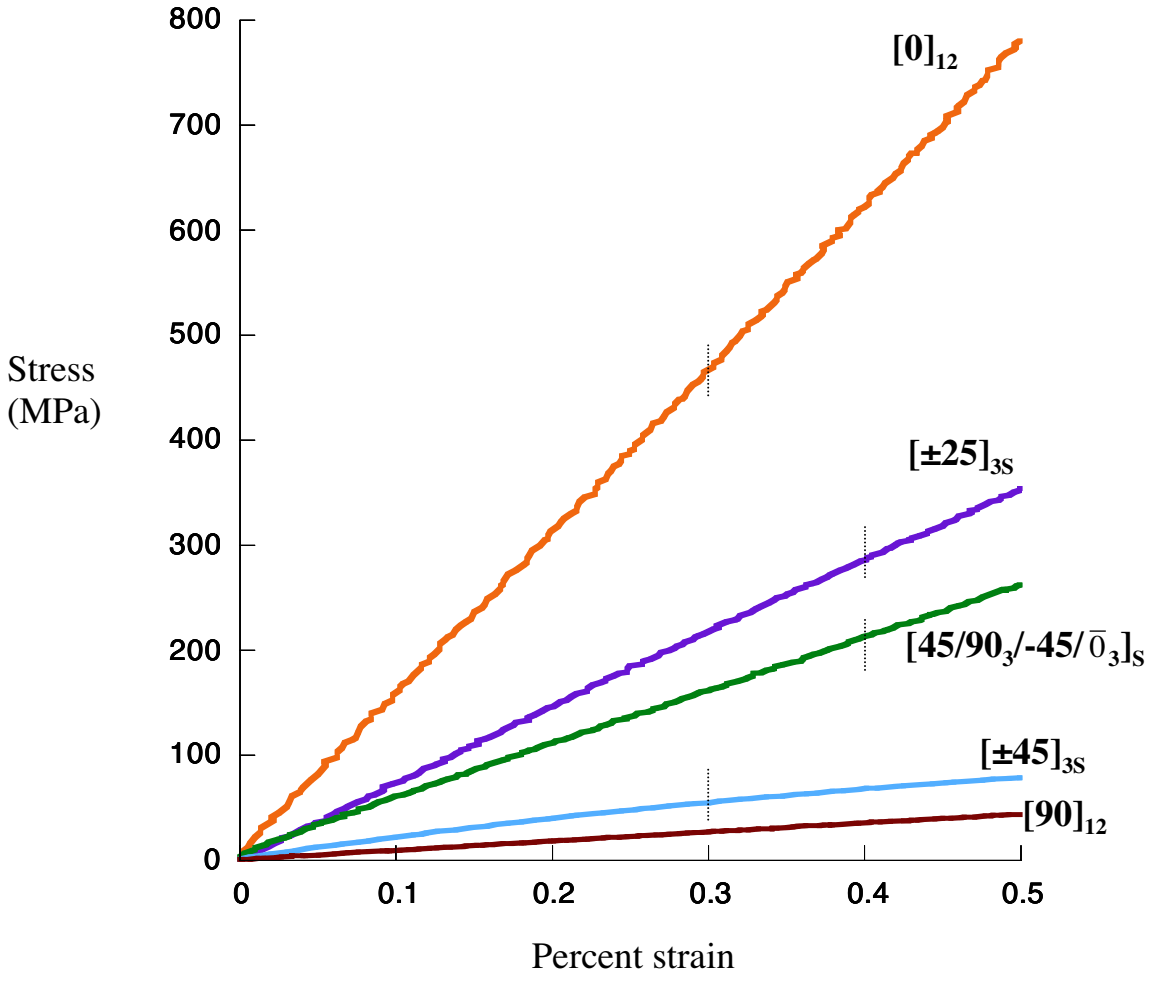

Figure 4. Stress-strain curves on a reduced scale with dotted-hash marks showing chosen pre-strain levels for each lay-up.

Figure 5. Cryogenic aging chamber.

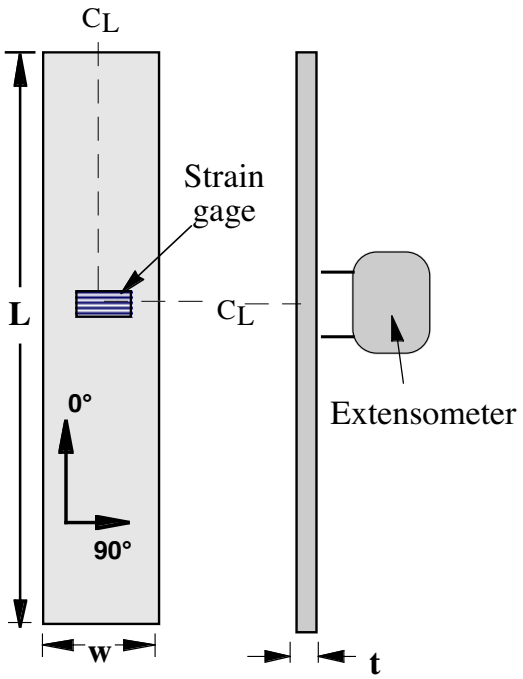

Test Temp.	w (mm)	L (mm)
24 °C	25.4	152.4
-196 °C	19.0	254.0
-269 °C	19.0	254.0

Figure 6. Schematic of tensile specimen. Thickness depends on specimen lay-up.

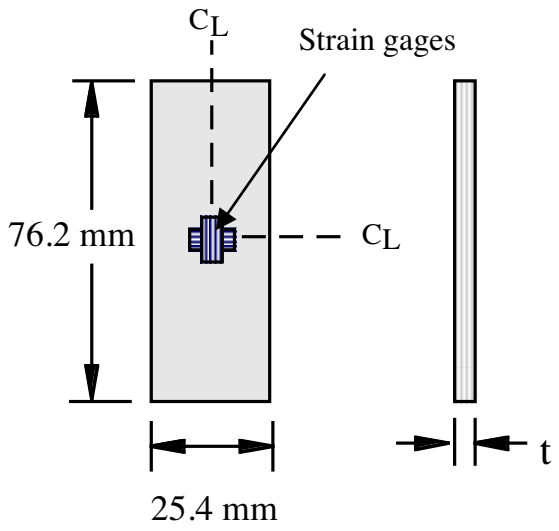

Figure 7. Schematic of compression specimen. Thickness depends on specimen lay-up.

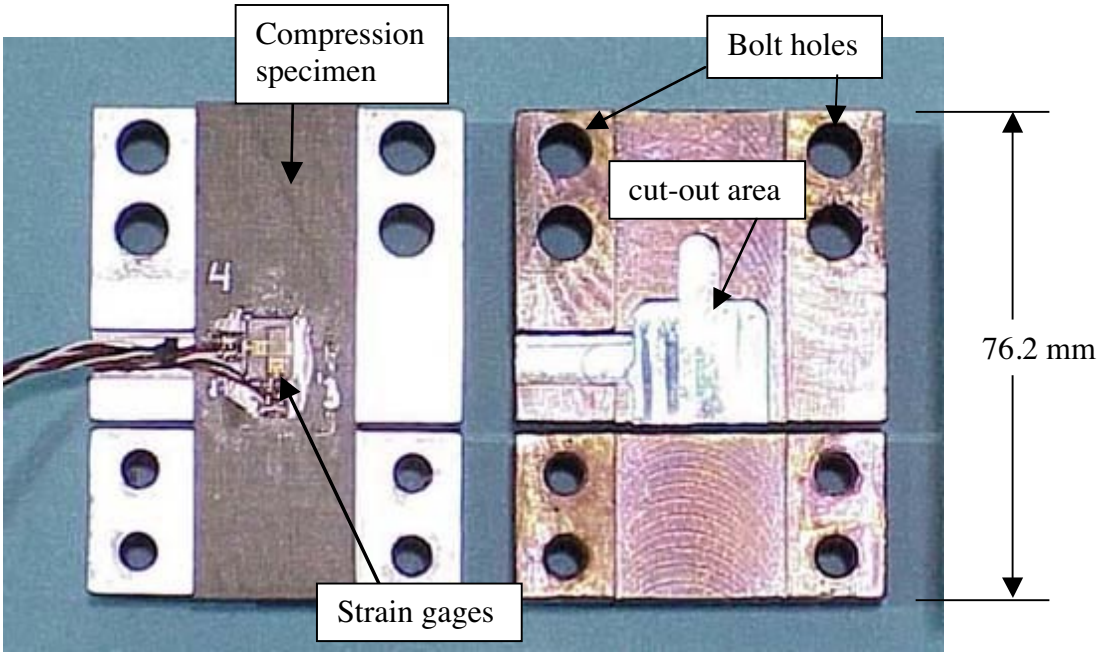

Figure 8(a). Compression test fixture open with specimen.

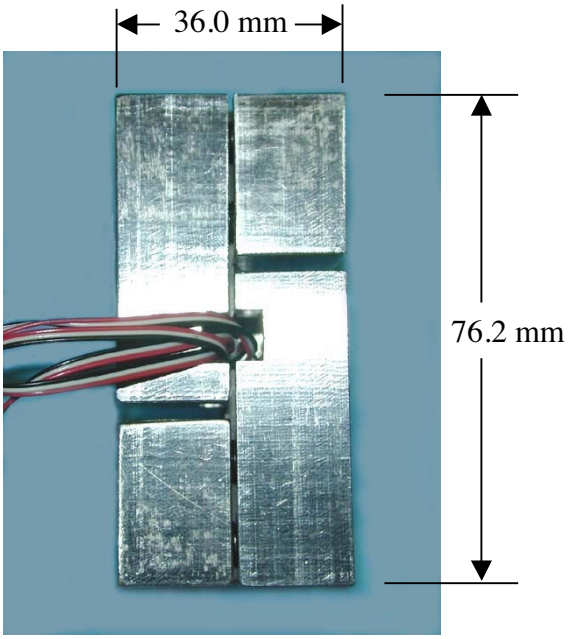

Figure 8(b). Side view of compression test fixture.

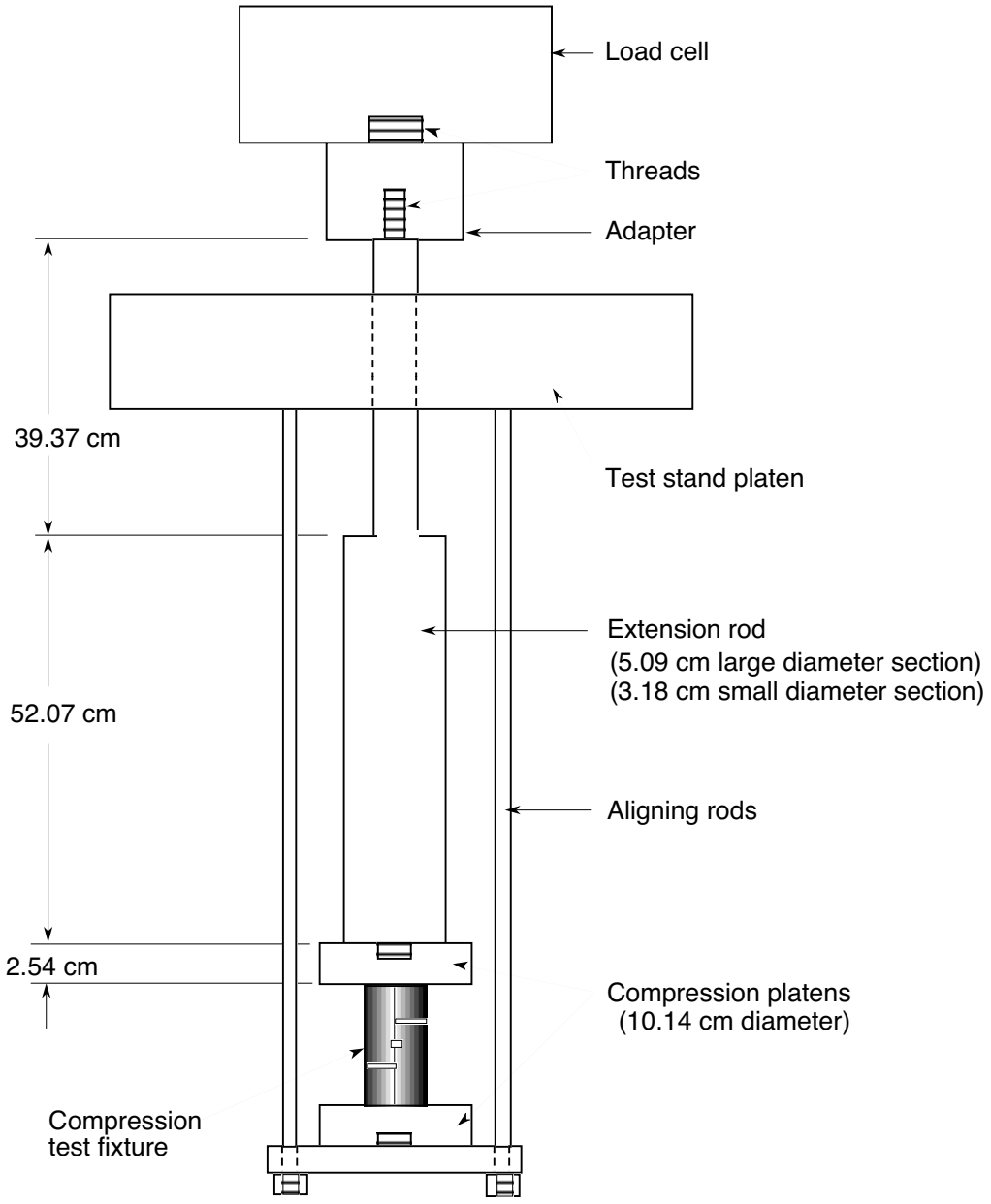

Figure 9. Schematic of apparatus set-up for compression test. Note: Drawing is not to scale.

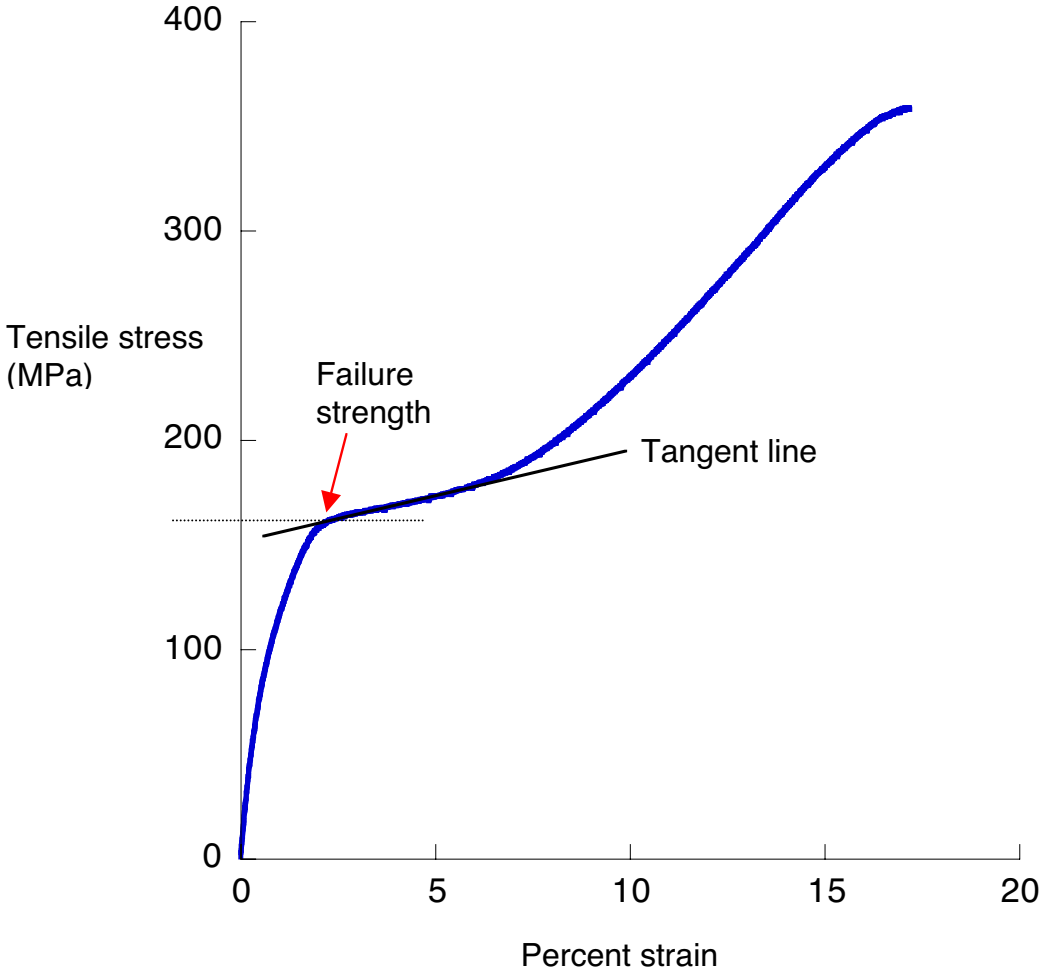

Figure 10. Room temperature stress-strain curve of $[\pm 45]_{3S}$–ply laminate in tension depicting the defined failure strength location at the intersection of the tangent line and the stress-strain curve.

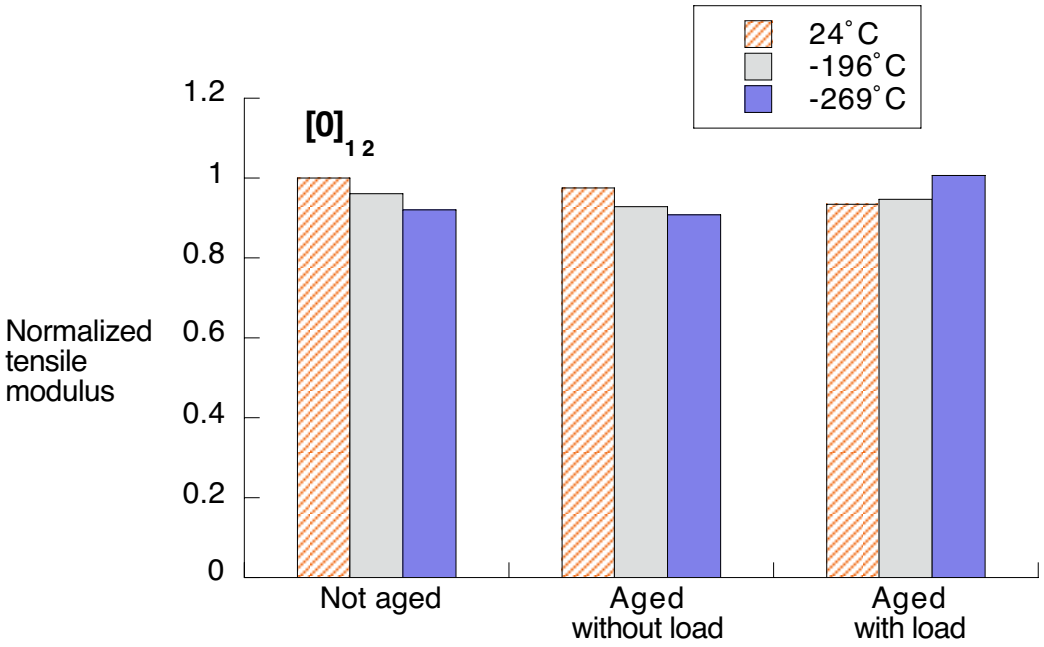

Figure 11. Tensile modulus of specimens with $[0]_{12}$ –ply laminate normalized against the not aged condition tested at room temperature.

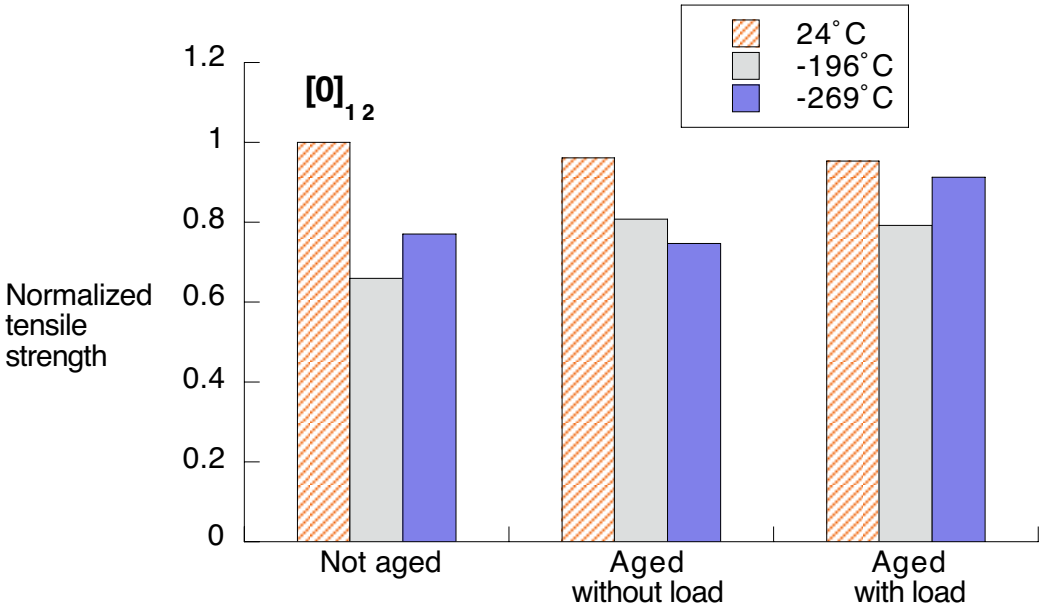

Figure 12. Tensile strength of specimens with $[0]_{12}$ –ply laminate normalized against the not aged condition tested at room temperature.

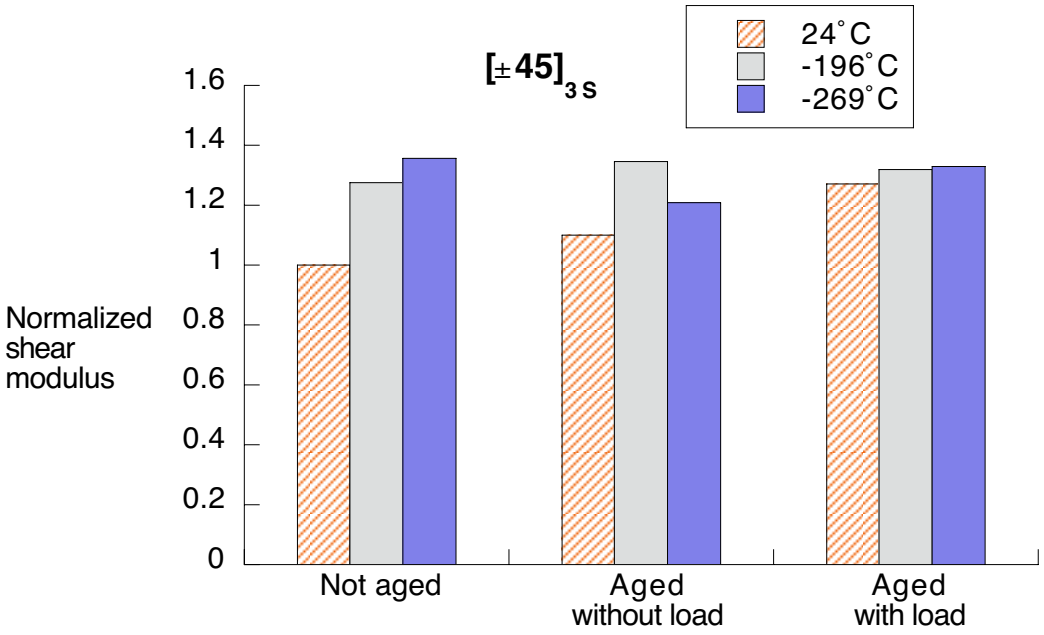

Figure 13. Shear tensile modulus of specimens with $[\pm 45]_{3S}$ –ply laminate normalized against the not aged condition tested at room temperature.

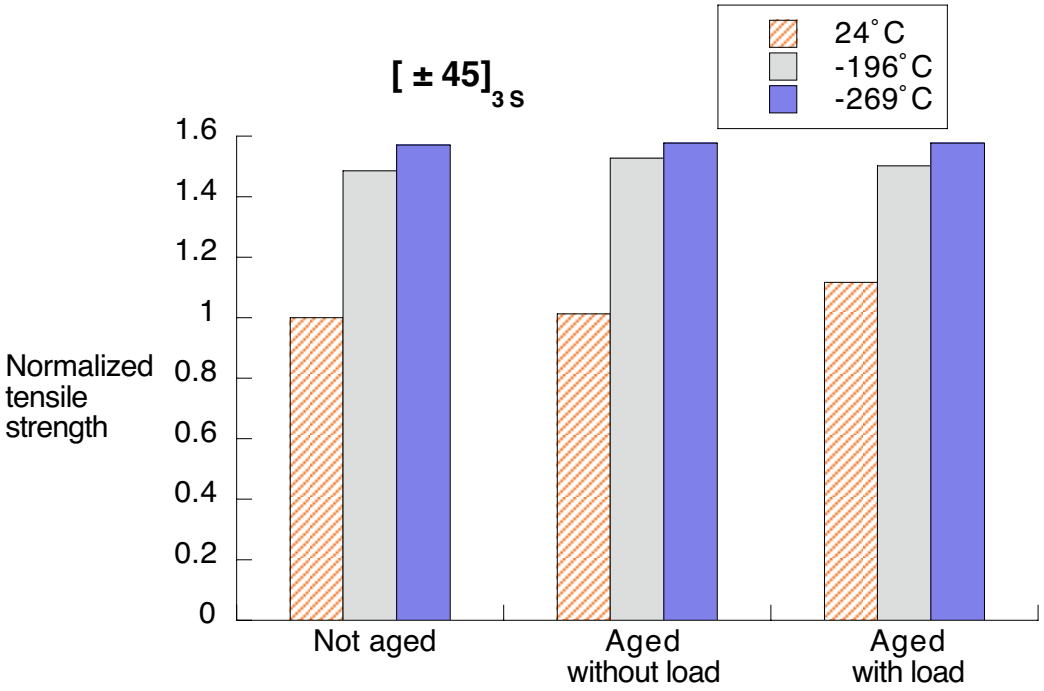

Figure 14. Tensile strength of specimens with $[\pm 45]_{3S}$ –ply laminate normalized against the not aged condition tested at room temperature.

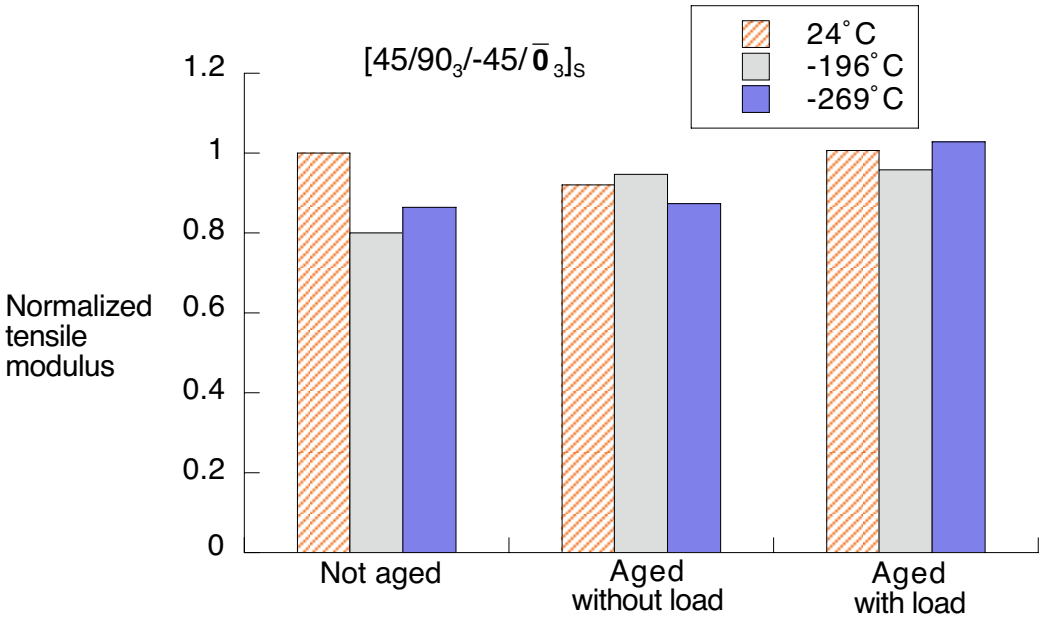

Figure 15. Tensile modulus of specimens with [45/90$_3$/-45/$\bar{0}_3$]$_S$ –ply laminate normalized against the not aged condition tested at room temperature.

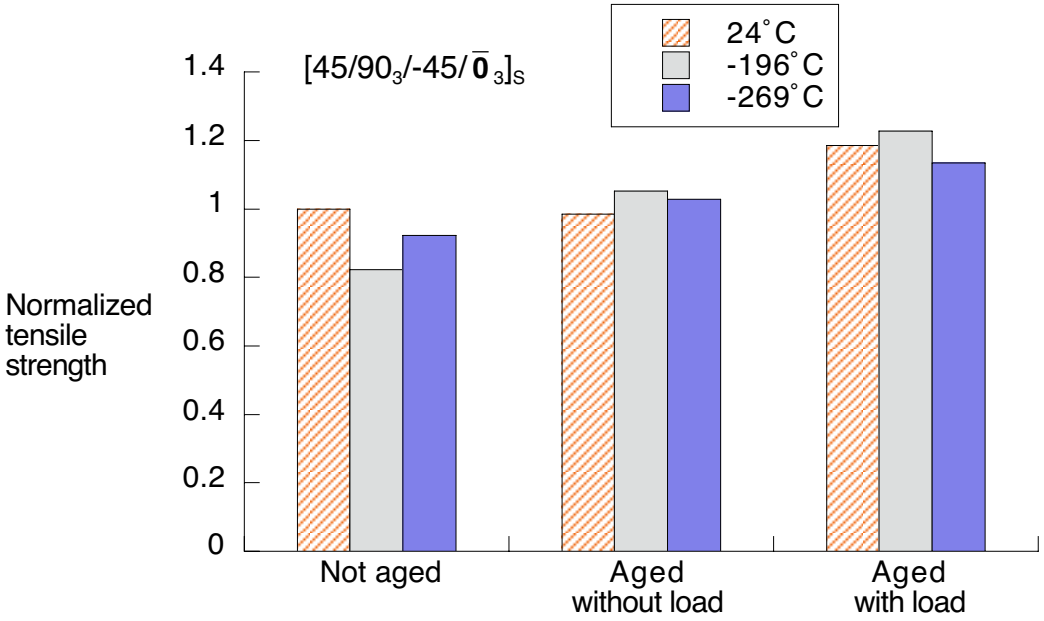

Figure 16. Tensile strength of specimens with [45/90$_3$/-45/$\bar{0}_3$]$_S$ –ply laminate normalized against the not aged condition tested at room temperature.

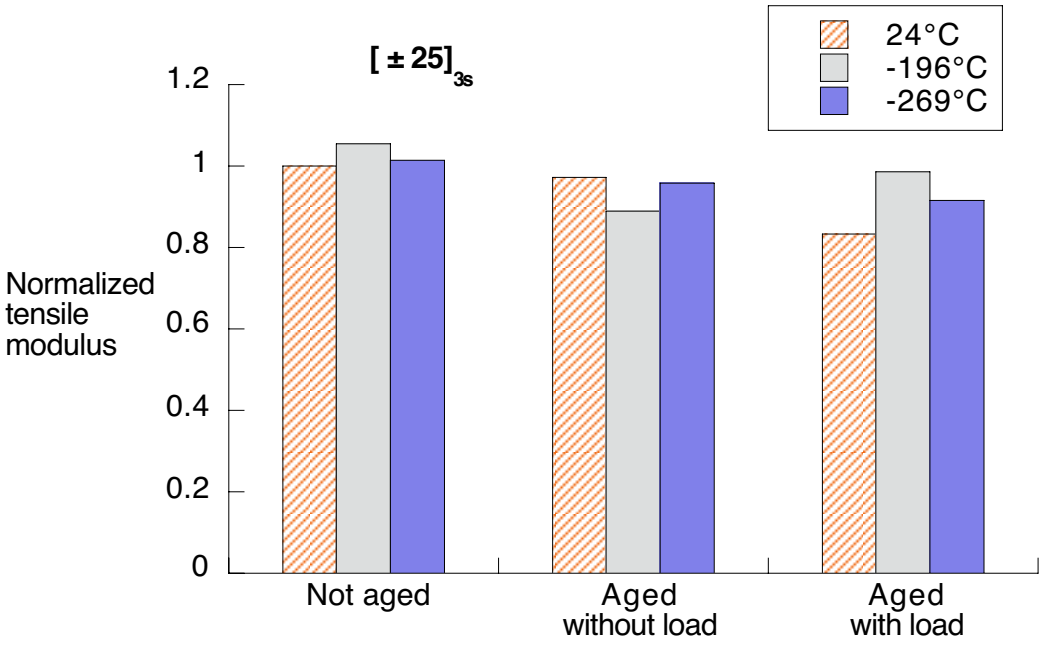

Figure 17. Tensile modulus of specimens with $[\pm 25]_{3S}$ –ply laminate normalized against the not aged condition tested at room temperature.

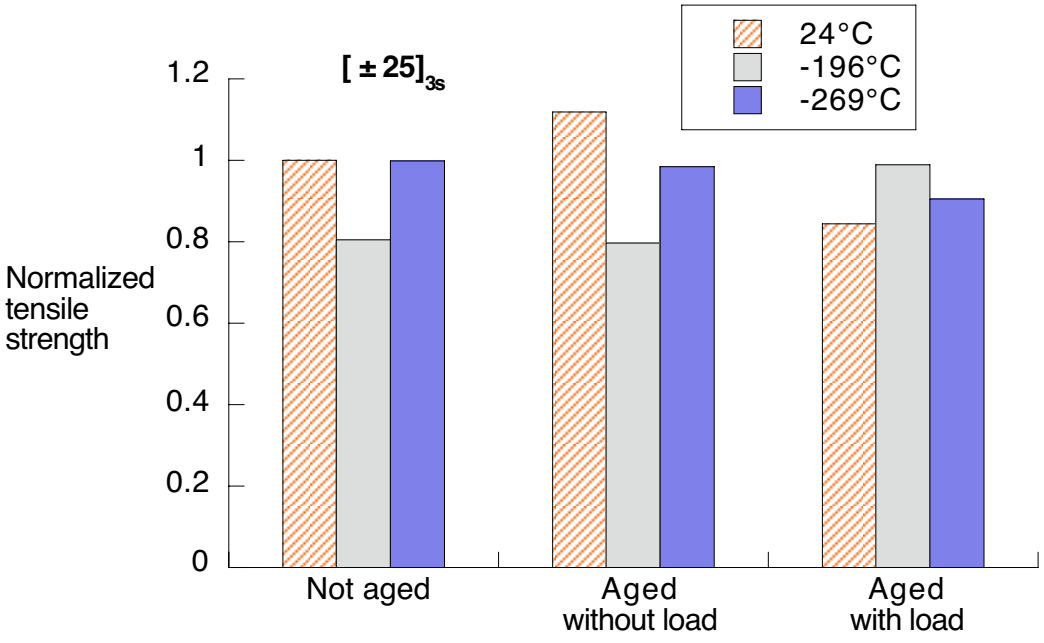

Figure 18. Tensile strength of specimens with $[\pm 25]_{3S}$ –ply laminate normalized against the not aged condition tested at room temperature.

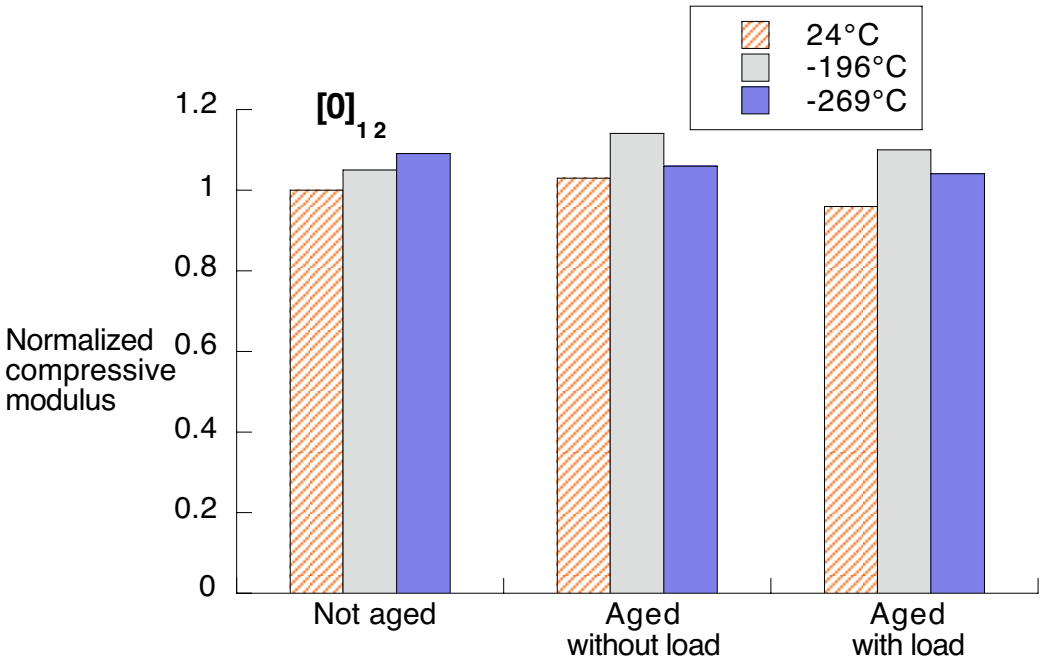

Figure 19. Compressive modulus of specimens with $[0]_{12}$ –ply laminate normalized against the not aged condition tested at room temperature.

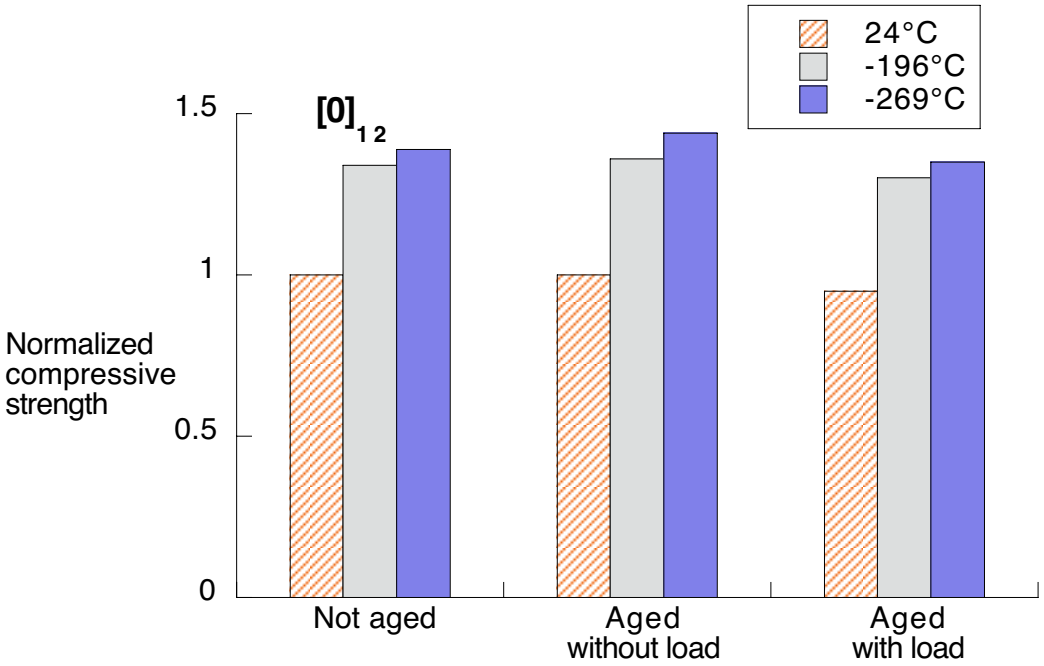

Figure 20. Compressive strength of specimens with $[0]_{12}$ –ply laminate normalized against the not aged condition tested at room temperature.

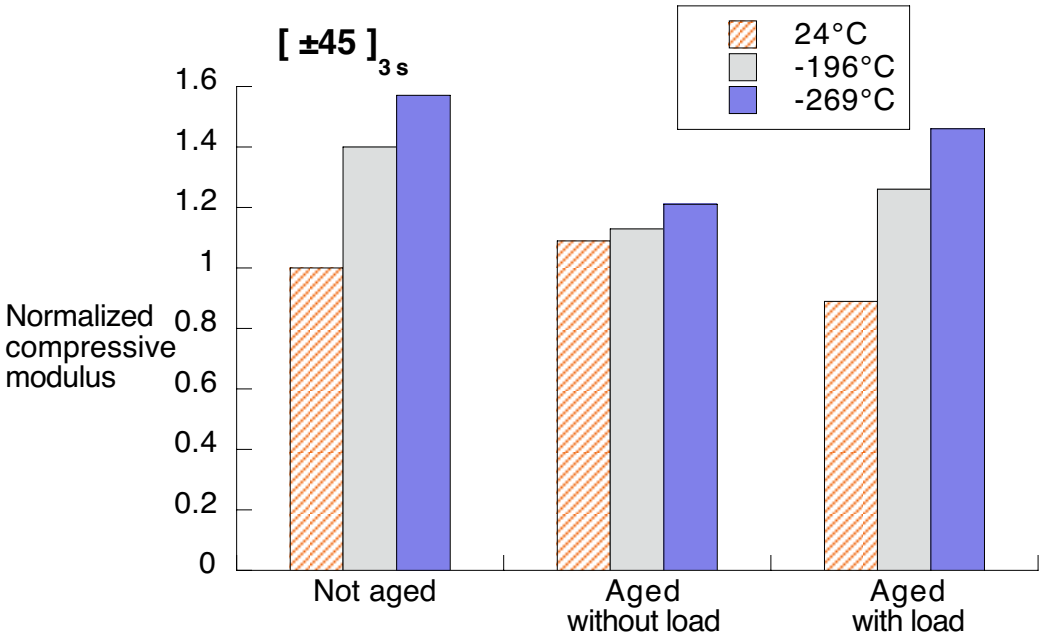

Figure 21. Compressive modulus of specimens with $[\pm 45]_{3s}$ –ply laminate normalized against the not aged condition tested at room temperature.

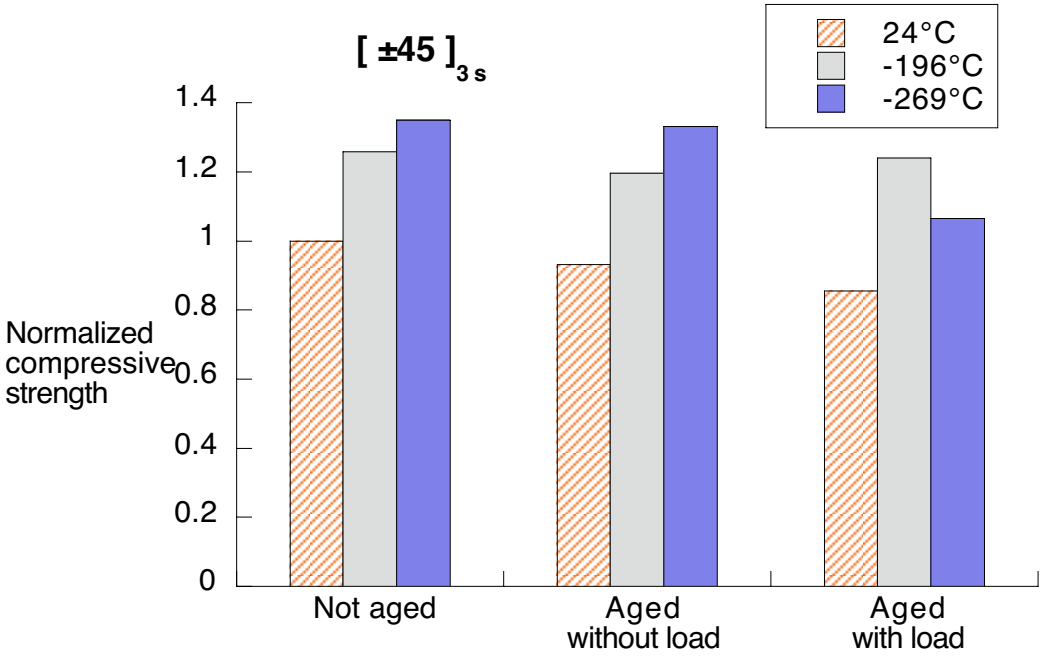

Figure 22. Compressive strength of specimens with $[\pm 45]_{3s}$ –ply laminate normalized against the not aged condition tested at room temperature.

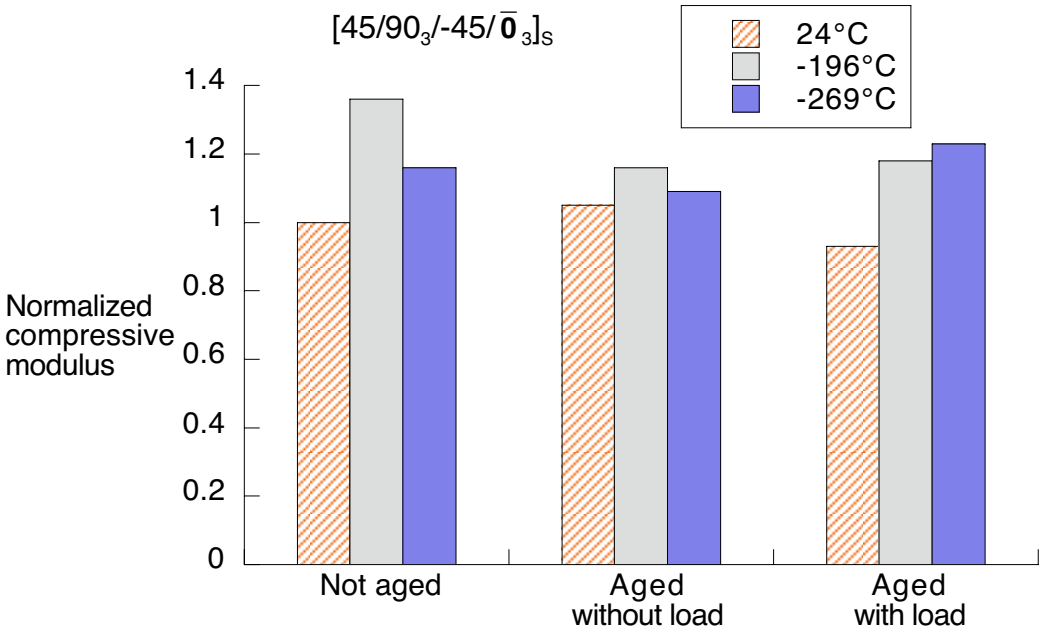

Figure 23. Compressive modulus of specimens with [45/90$_3$/-45/$\bar{0}_3$]$_S$ –ply laminate normalized against the not aged condition tested at room temperature.

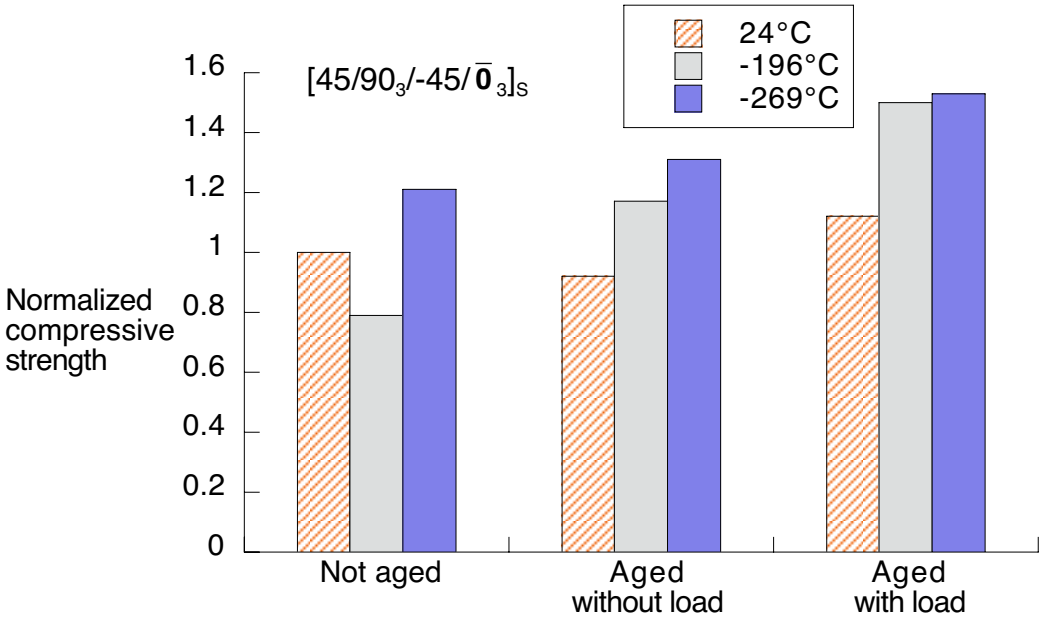

Figure 24. Compressive strength of specimens with [45/90$_3$/-45/$\bar{0}_3$]$_S$ –ply laminate normalized against the not aged condition tested at room temperature.

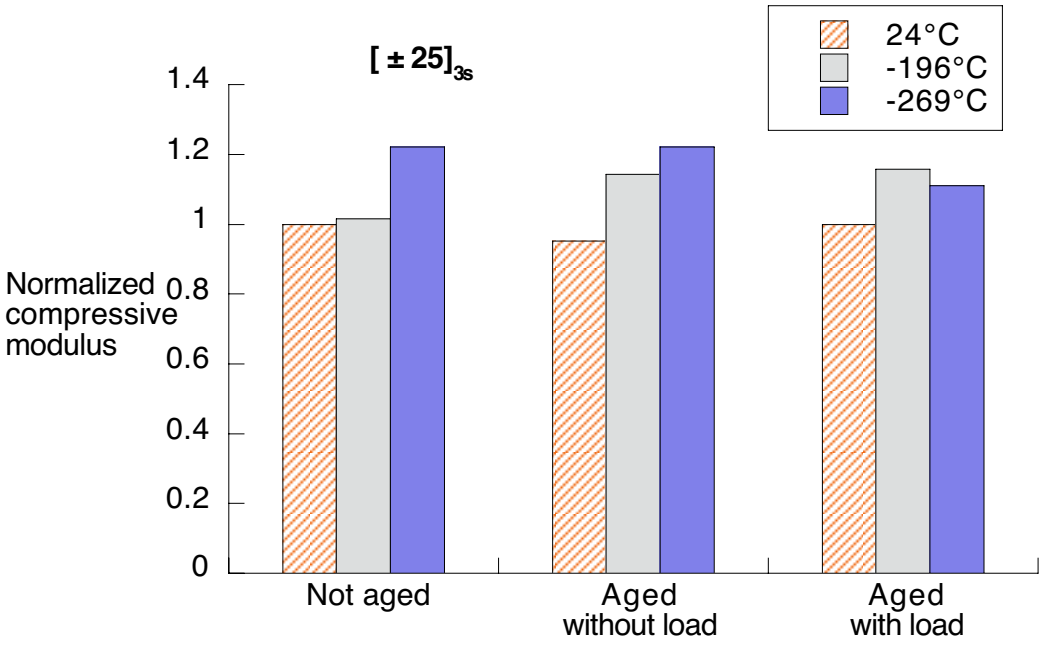

Figure 25. Compressive modulus of specimens with $[\pm 25]_{3S}$ –ply laminate normalized against the not aged condition tested at room temperature.

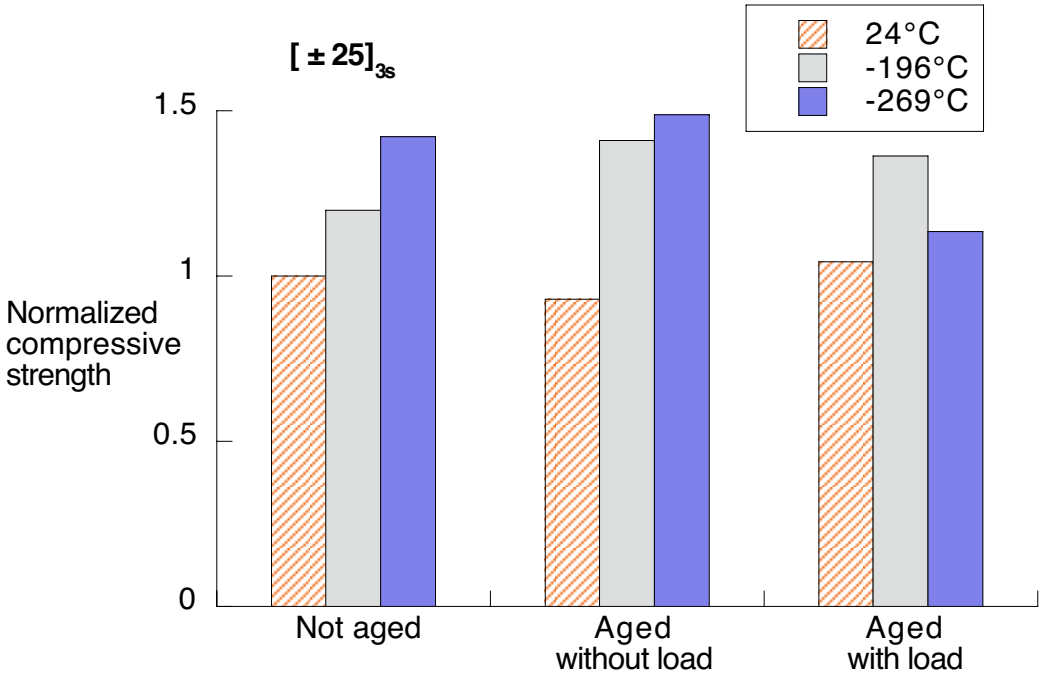

Figure 26. Compressive strength of specimens with $[\pm 25]_{3S}$ –ply laminate normalized against the not aged condition tested at room temperature.

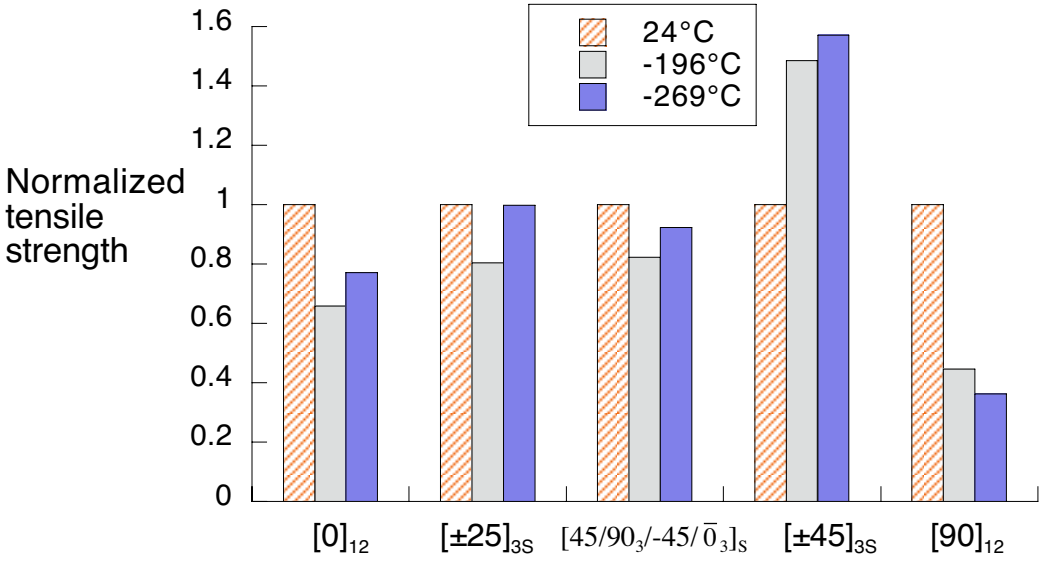

Figure 27. Tensile strength of not-aged material normalized against the room temperature test within each laminate group.

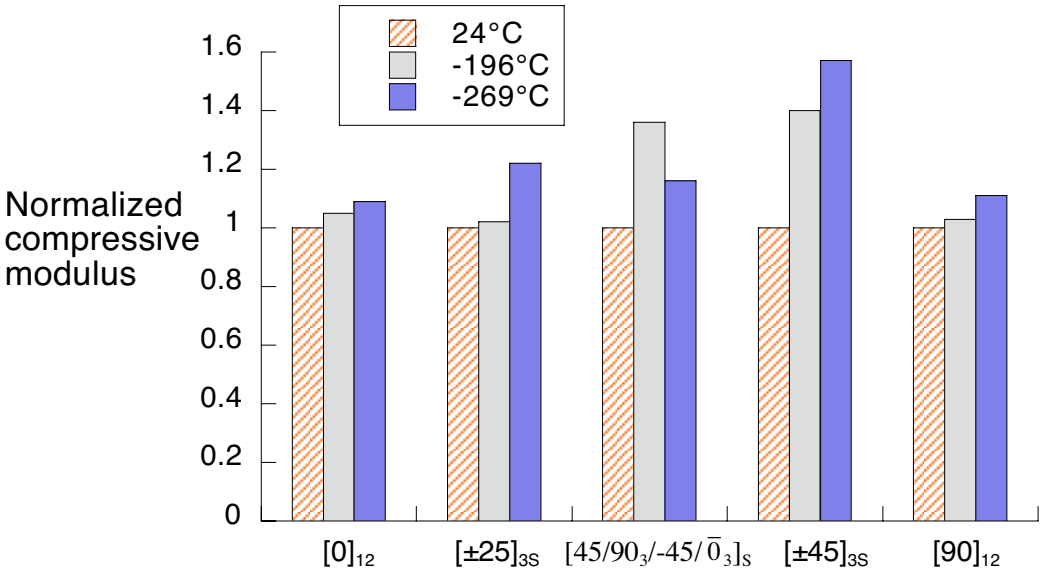

Figure 28. Compressive modulus of not-aged material normalized against room temperature test within each laminate group.

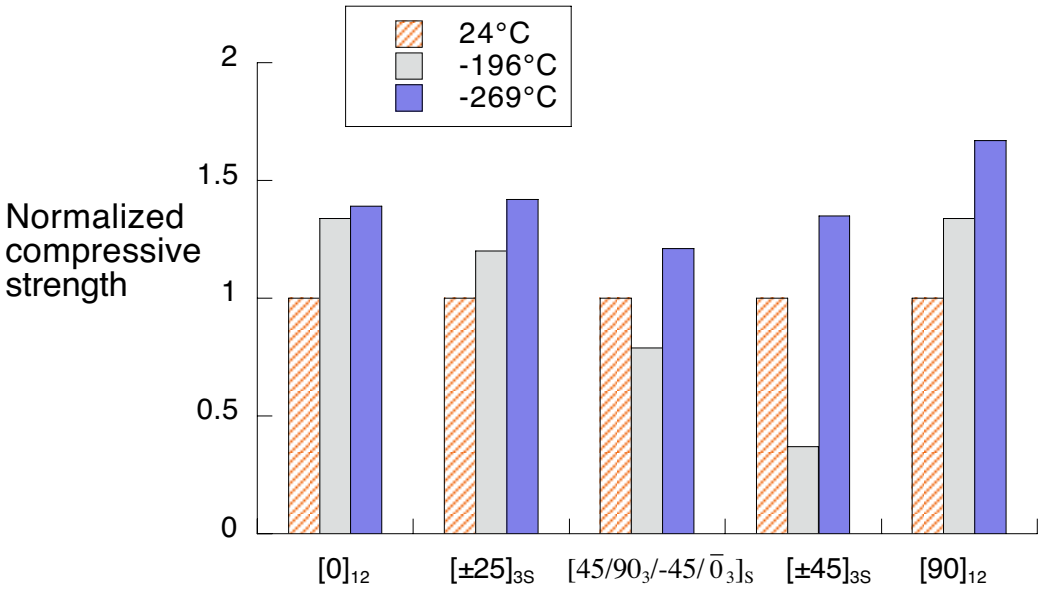

Figure 29. Compressive strength of not-aged material normalized against room temperature test within each laminate group.

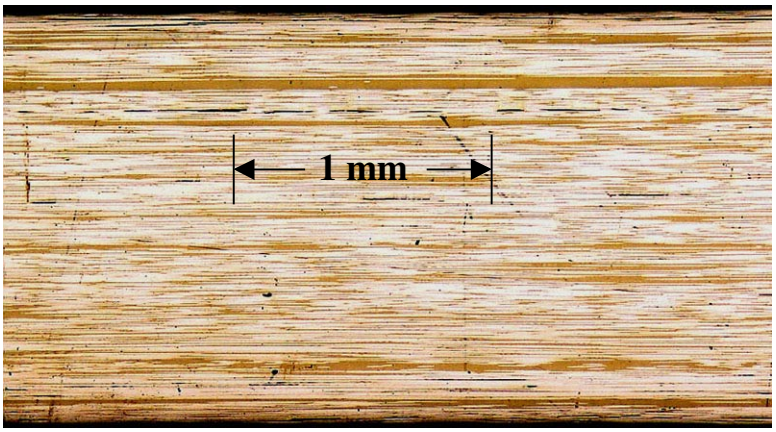

Figure 30(a). Photomicrograph (25x) of edge of $[0]_{12}$ not aged.

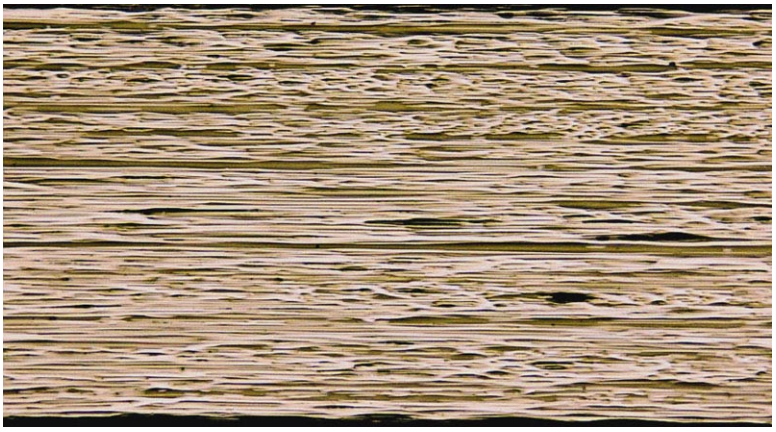

Figure 30(b). Photomicrograph (25x) of edge of $[0]_{12}$ aged without load.

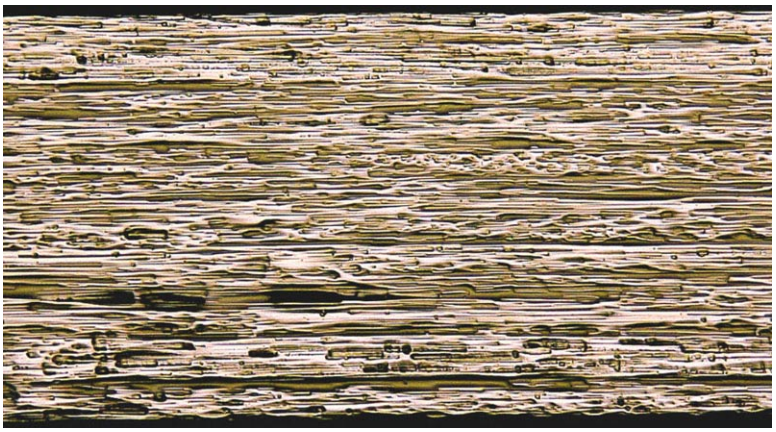

Figure 30(c). Photomicrograph (25x) of edge of $[0]_{12}$ aged with load.

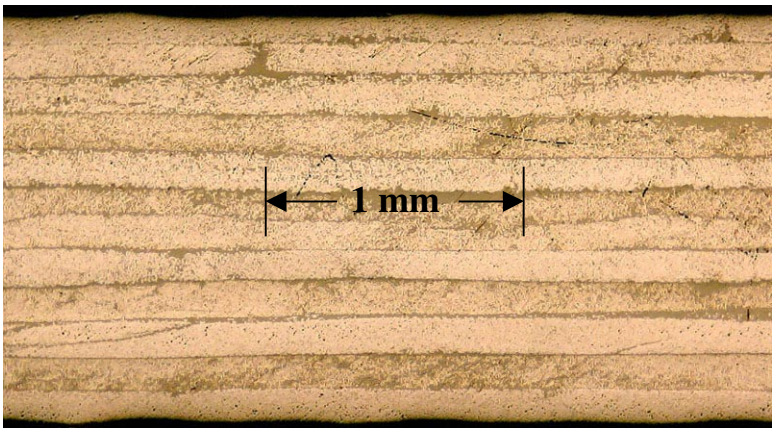

Figure 31(a). Photomicrograph (25x) of edge of $[\pm 45]_{3S}$ not aged.

Figure 31(b). Photomicrograph (25x) of edge of $[\pm 45]_{3S}$ aged without load.

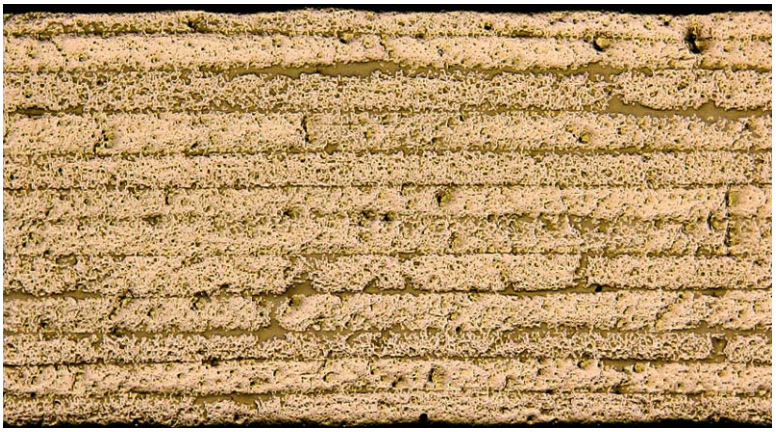

Figure 31(c). Photomicrograph (25x) of edge of $[\pm 45]_{3S}$ aged with load.

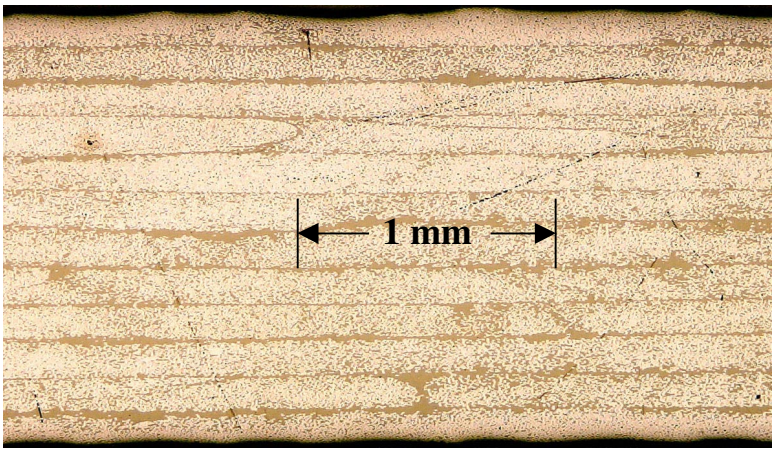

Figure 32(a). Photomicrograph (25x) of edge of $[\pm 25]_{3S}$ not aged.

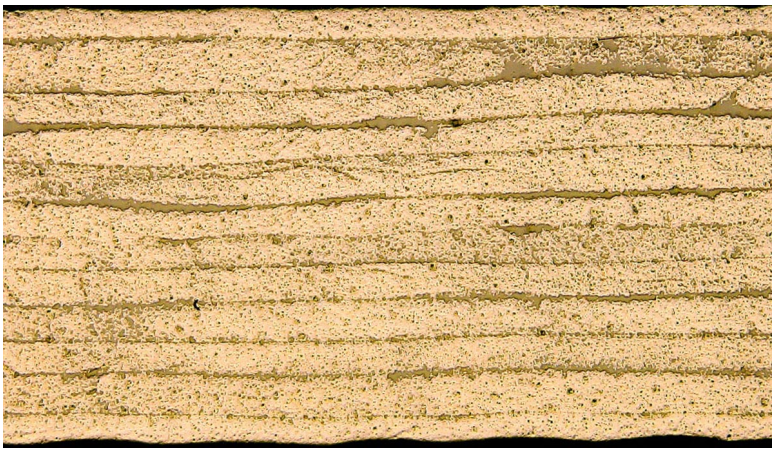

Figure 32(b). Photomicrograph (25x) of edge of $[\pm 25]_{3S}$ aged without load.

Figure 32(c). Photomicrograph (25x) of edge of $[\pm 25]_{3S}$ aged with load.

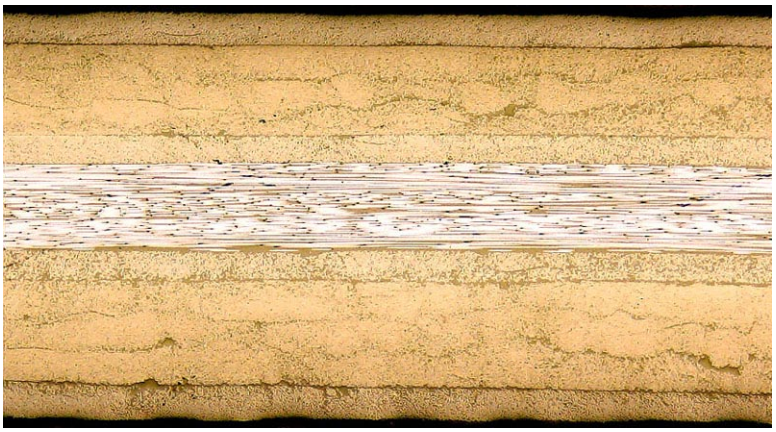

Figure 33(a). Photomicrograph (25x) of edge of $[45/90_3/\text{-}45/\bar{0}_3]_S$ not aged.

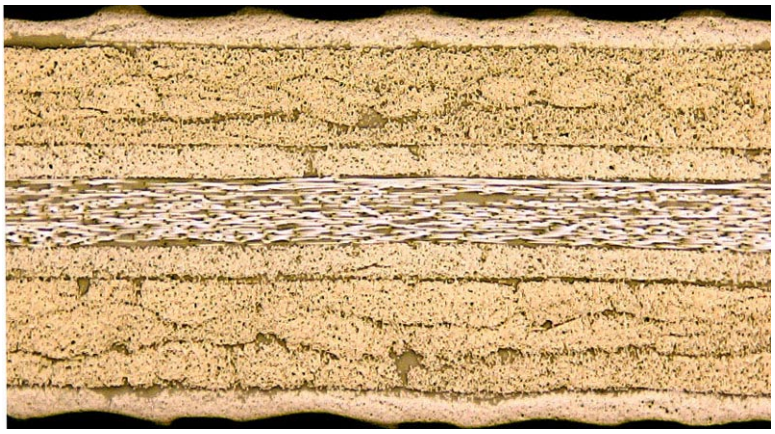

Figure 33(b). Photomicrograph (25x) of edge of $[45/90_3/\text{-}45/\bar{0}_3]_S$ aged without load.

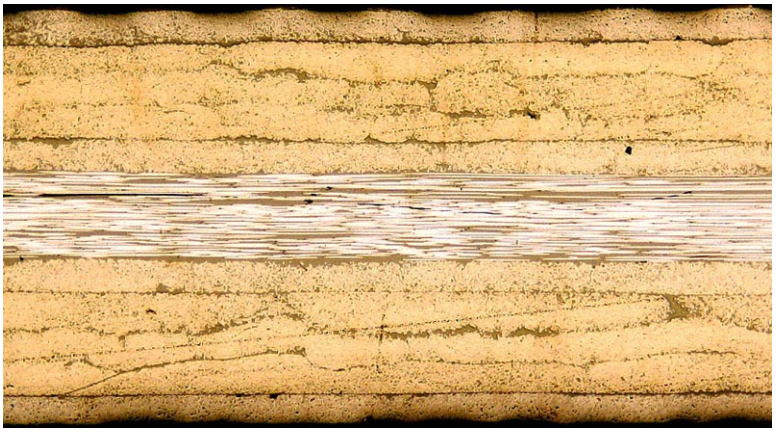

Figure 33(c). Photomicrograph (25x) of edge of $[45/90_3/\text{-}45/\bar{0}_3]_S$ aged with load.

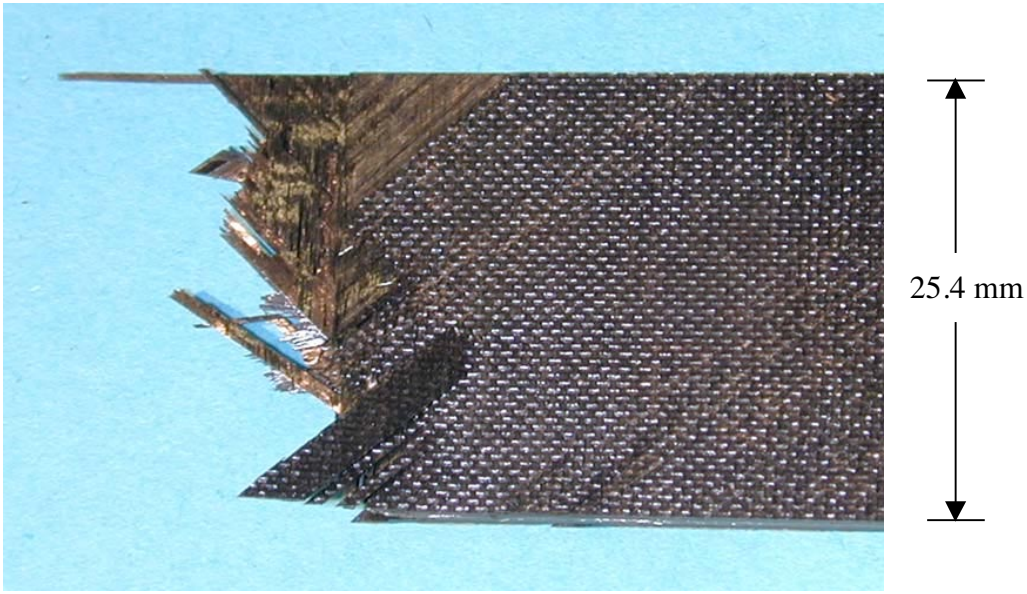

Figure 34(a). Fracture surface of $[45/90_3/\text{-}45/\bar{0}_3]_S$ –ply laminate after tension test at room temperature.

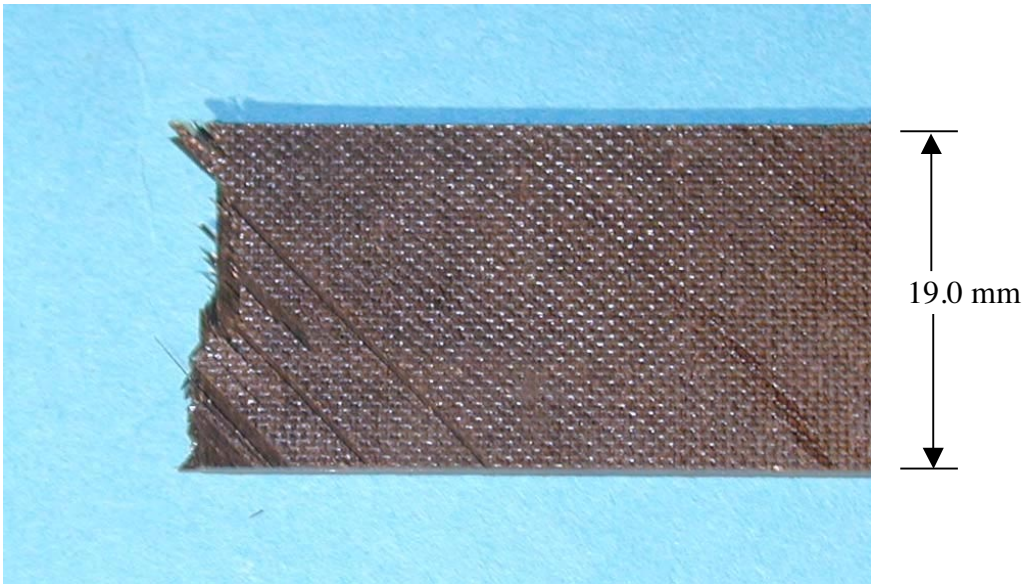

Figure 34(b). Fracture surface of $[45/90_3/\text{-}45/\bar{0}_3]_S$ –ply laminate after tension test at –196°C.

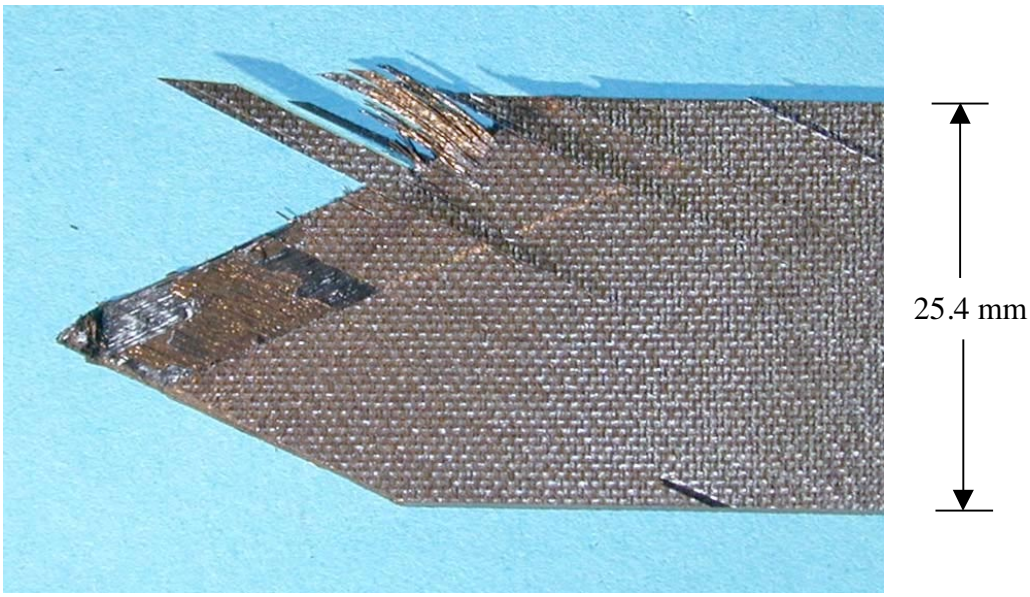

Figure 35(a). Fracture surface of $[\pm 25]_{3S}$ –ply laminate after tension test at room temperature.

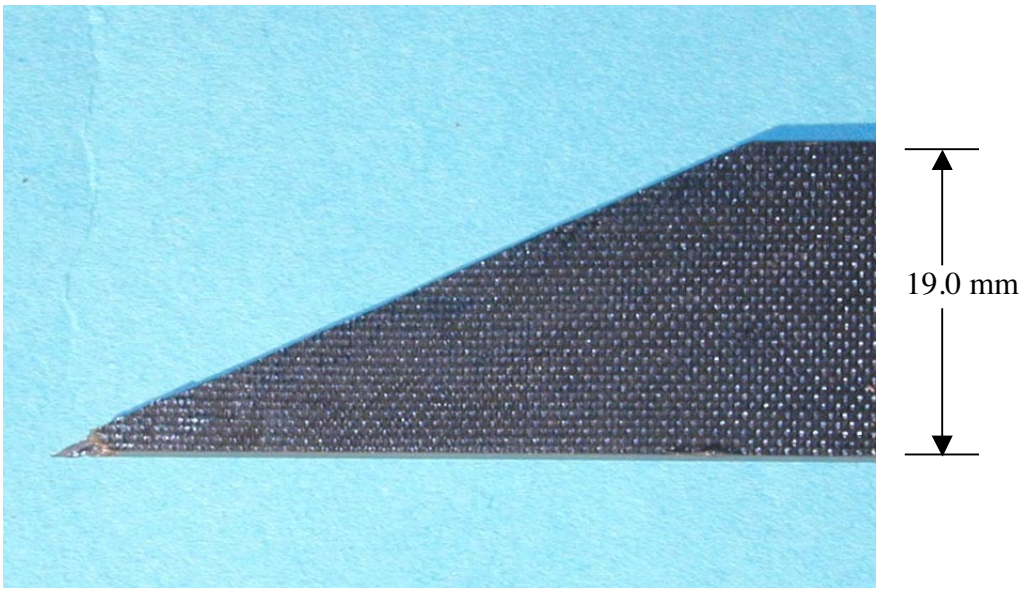

Figure 35(b). Fracture surface of $[\pm 25]_{3S}$ –ply laminate after tension test at –196°C.

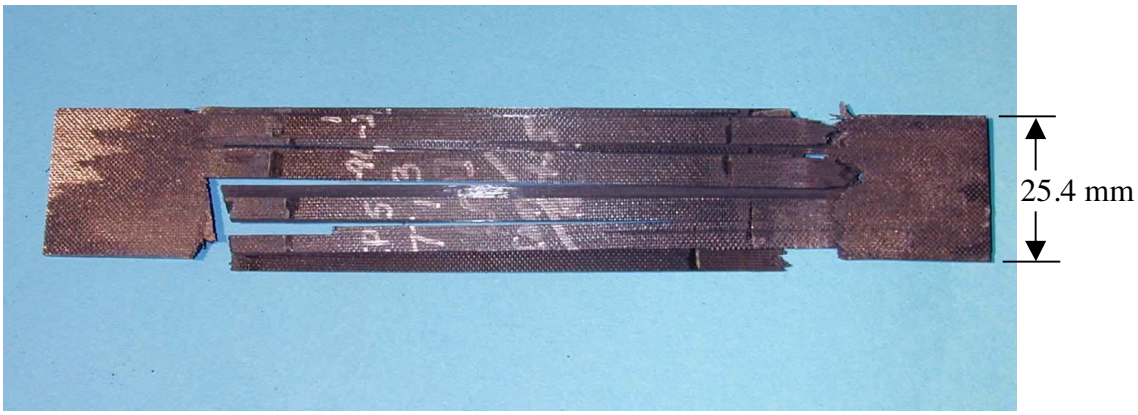

Figure 36(a). Fracture surface of $[0]_{12}$–ply laminate after tension test at room temperature.

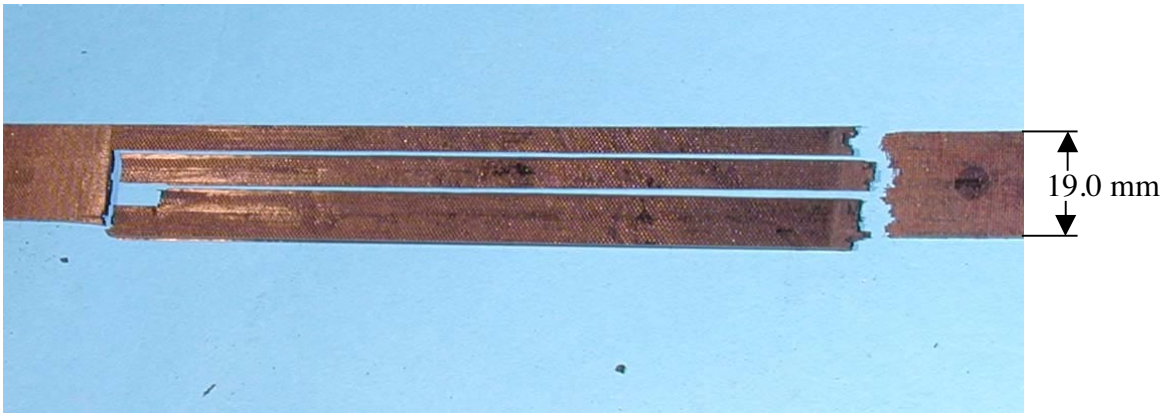

Figure 36(b). Fracture surface of $[0]_{12}$–ply laminate after tension test at –196°C.

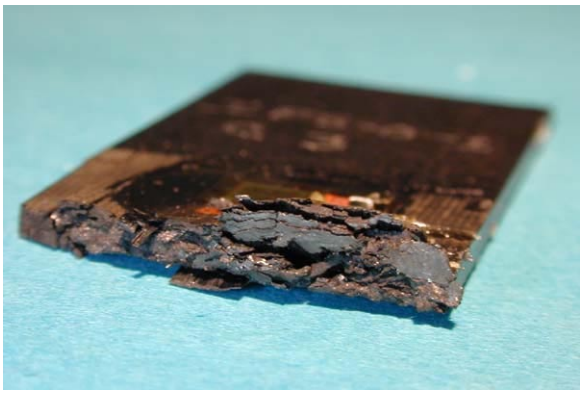

Figure 37. Fracture surface of $[0]_{12}$ –ply laminate after compression test at room temperature.

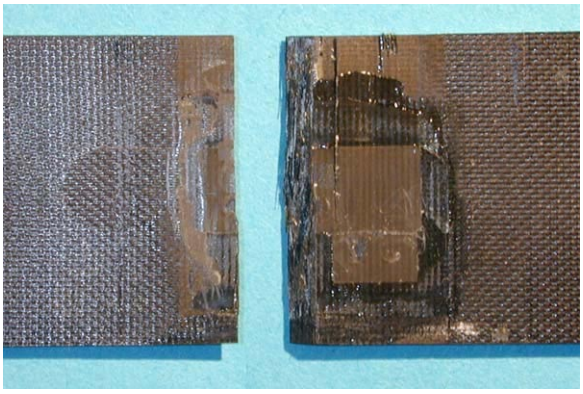

Figure 38. Fracture surface of $[90]_{12}$ –ply laminate after compression test at room temperature.

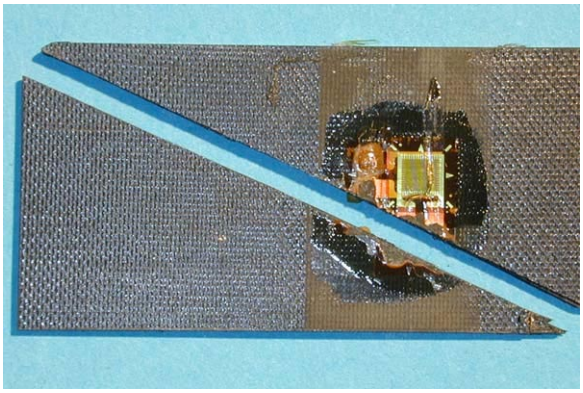

Figure 39. Fracture surface of $[\pm 25]_{3S}$ –ply laminate after compression test at room temperature.

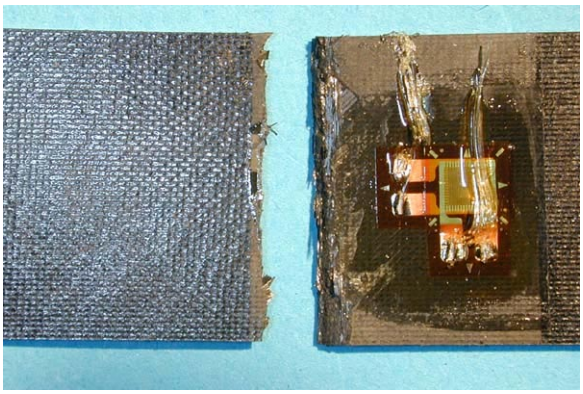

Figure 40. Fracture surface of $[45/90_3/-45/\bar{0}_3]_S$ –ply laminate after compression test at room temperature.

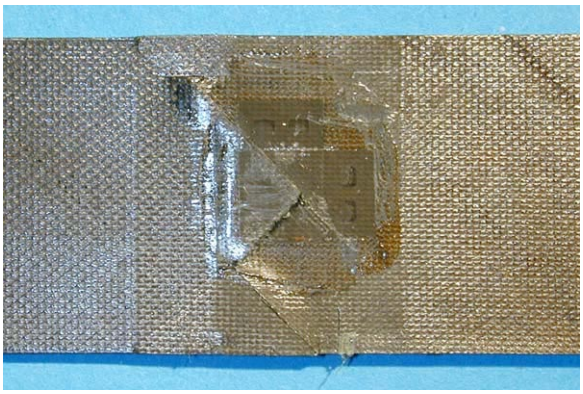

Figure 41(a). Fracture surface of $[\pm 45]_{3S}$ –ply laminate after compression test at room temperature.

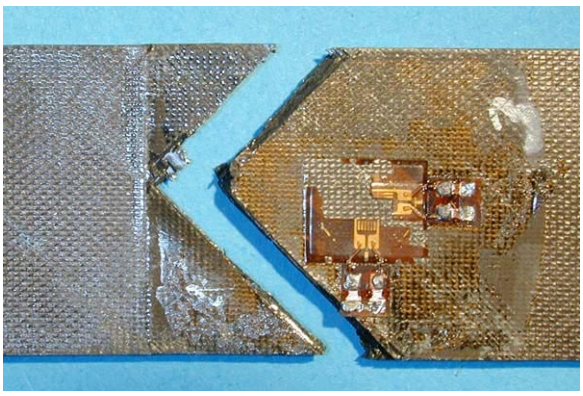

Figure 41(b). Fracture surface of $[\pm 45]_{3S}$ –ply laminate after compression test at –196°C.

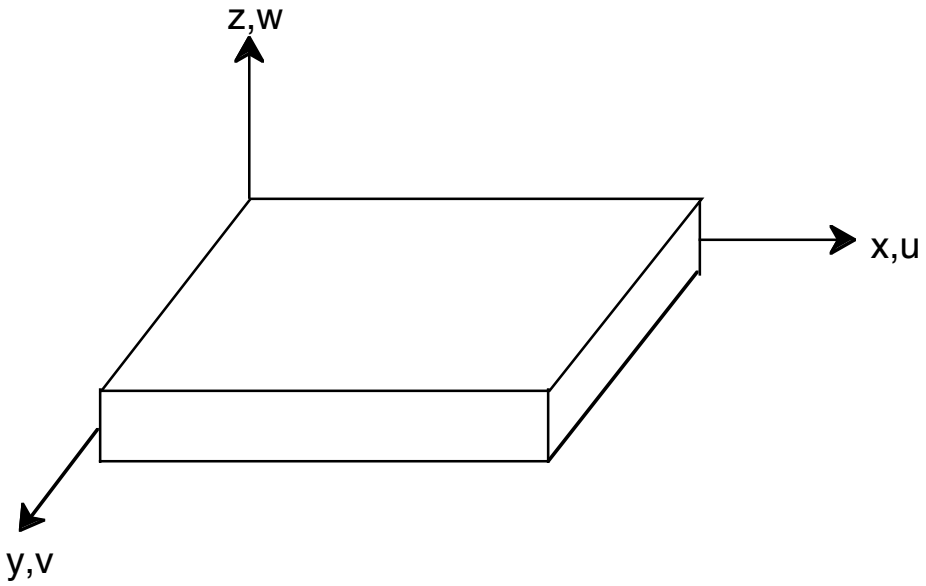

Figure 42. Displacements u, v, w in the x, y, z directions.

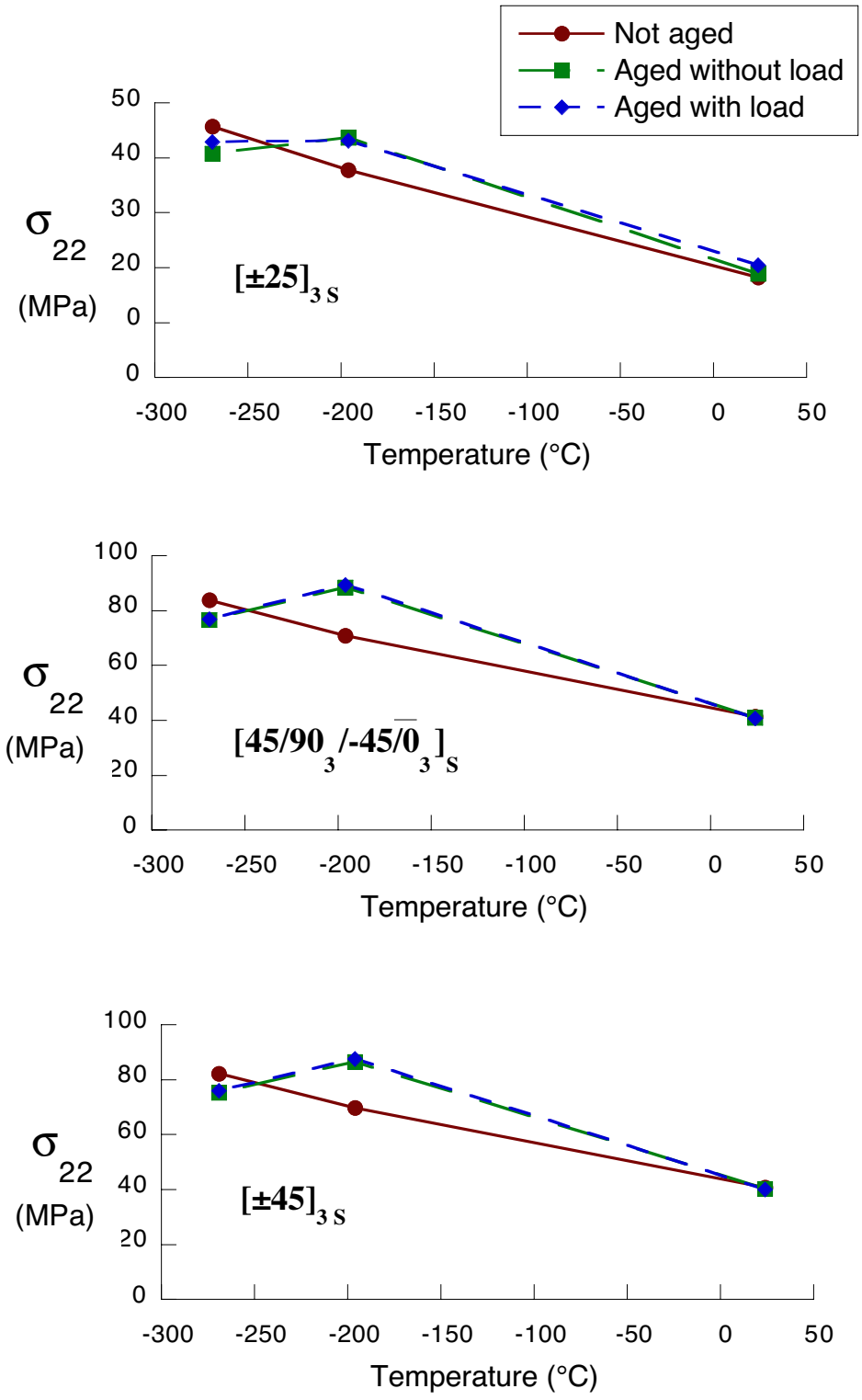

Figure 43. Maximum transverse ply stress for the thermal loading only, calculated using tensile modulus values.

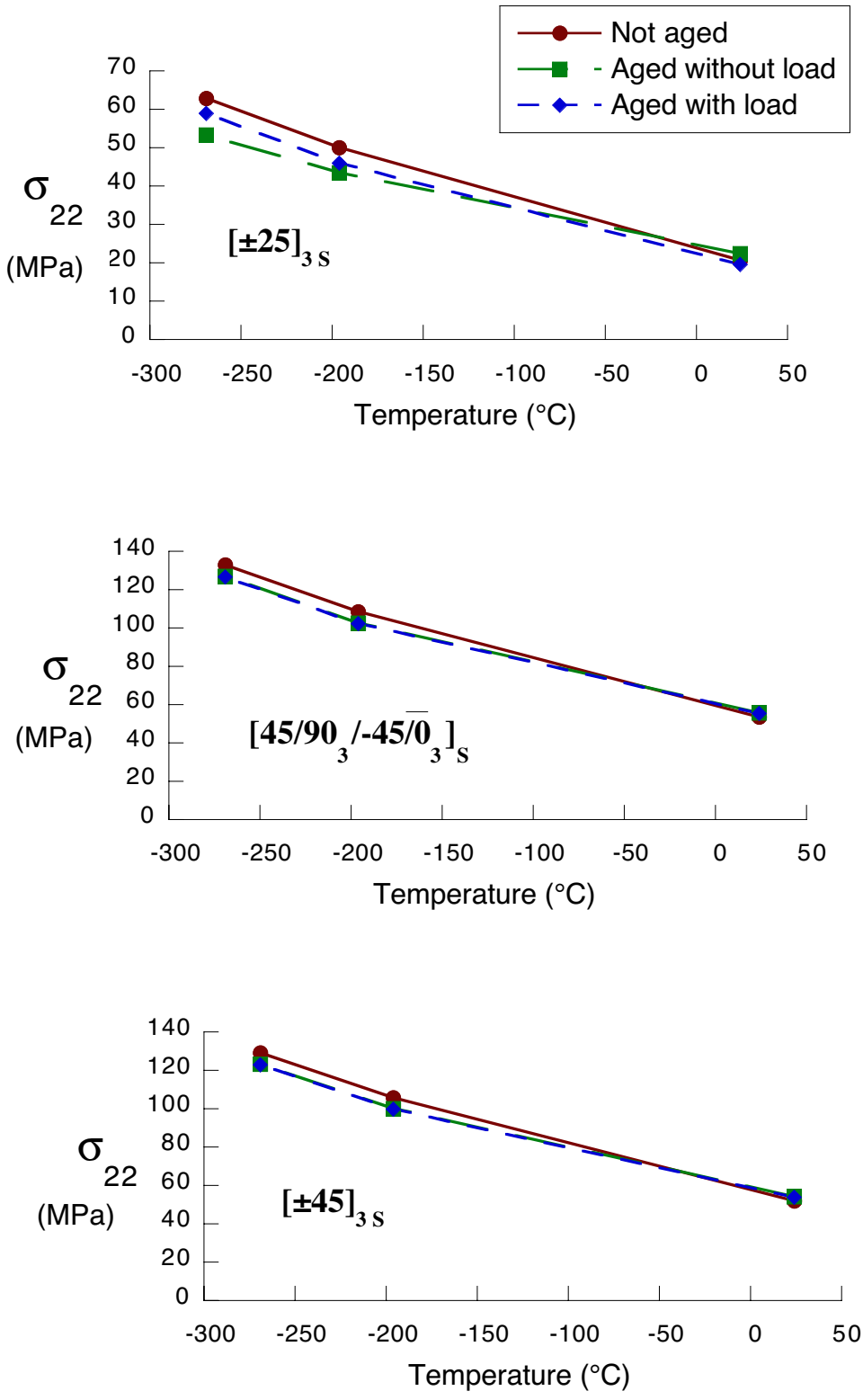

Figure 44. Maximum transverse ply stress as a function of temperature for thermal loading only, calculated using compressive modulus

VITA

In the second half of the twentieth century, Karen Suzanne Morgan Whitley was born to loving parents, Arthur Lee and Mary Madeline Morgan of Yorktown, Virginia. Karen attended Seaford Elementary, Yorktown Intermediate, and graduated from York High School. She married the charming Richard Thomas Whitley while attending Thomas Nelson Community College, and she graduated with an Associate in Applied Science degree in Mechanical Engineering Technology. She accepted a position as a mechanical engineer technician at NASA Langley Research Center and graduated from their Apprenticeship Program. One year prior to the apprenticeship graduation, Karen gave birth to an energetic son named Justin, and six years later, she gave birth to a spirited daughter named Megan. She went on to obtain a Bachelor of Science degree in Mathematics/Physics from Christopher Newport University, and then accepted a new position at NASA Langley Research Center as an aerospace engineer in the Materials Division, now known as the Structures and Materials Competency. Karen began pursuing a Masters degree in Engineering Mechanics from Virginia Polytechnic Institute and State University through the Virginia Consortium of Engineering and Science Universities, and will graduate in December 2002. Yippy, Ye-ha!!